Exhumation tectonics of the ultrahigh-pressure metamorphic rocks in the Qinling orogen in east China: New petrological-structural-radiometric insights from the Shandong Peninsula

Michel Faure, Wei Lin, Patrick Monié, Nicole Le Breton, Stéphane Poussineau, Dominique Panis, Etienne Deloule

Exhumation tectonics of the ultrahigh-pressure metamorphic rocks in the Qinling orogen in east China: New petrological-structural-radiometric insights from the Shandong Peninsula

Michel Faure,[1] Wei Lin,[2] Patrick Monié,[3] Nicole Le Breton,[1] Stéphane Poussineau,[1] Dominique Panis,[1] and Etienne Deloule[4]

Received 20 August 2002; revised 21 December 2002; accepted 13 February 2003; published 17 May 2003.

[1] In eastern China, the Sulu area is recognized as the eastern extension of the Qinling-Dabie Belt, which is famous for its ultrahigh-pressure (UHP) metamorphism. Although numerous petrologic and geochemical works are available, structural data are still rare. This paper provides the first extensive study of bulk geometry and kinematic analysis of the Shandong Peninsula. The study area is divided into three tectonic areas by Cretaceous faults, namely, a southern UHP belt or Sulu area, a northern migmatite area, and an eastern eclogite and migmatite area or Weihai area. Conversely to the deeply entrenched idea that the later area belongs to the North China Belt, and the two others to the South China Block (SCB), we argue that all three areas are parts of the SCB. Structural, petrologic, $^{40}Ar/^{39}Ar$, and U/Pb data comply with this new interpretation. In the North Shandong area, mafic granulites enclosed as blocks within gneissic migmatites do not significantly differ from the Sulu and Weihai eclogites which also experienced a granulite facies overprint before migmatization. The circa 210–200 Ma age of the main ductile deformation is related to an extensional event during the Triassic (or Indosinian) orogeny. This date corresponds to the temperature climax, but the time of the pressure peak, i.e., the real age of the UHP metamorphism is discussed. *INDEX TERMS:* 8109 Tectonophysics: Continental tectonics—extensional (0905); 1035 Geochemistry: Geochronology; 3660 Mineralogy and Petrology: Metamorphic petrology; 9609 Information Related to Geologic Time: Mesozoic; 9320 Information Related to Geographic Region: Asia; *KEYWORDS:* ultrahigh-pressure metamorphism, granulite, migmatite, $^{40}Ar/^{39}Ar$ dating, ductile deformation, east China. **Citation:** Faure, M., W. Lin, P. Monié, N. Le Breton, S. Poussineau, D. Panis, and E. Deloule, Exhumation tectonics of the ultrahigh-pressure metamorphic rocks in the Qinling orogen in east China: New petrological-structural-radiometric insights from the Shandong Peninsula, *Tectonics*, *22*(3), 1018, doi:10.1029/2002TC001450, 2003.

1. Introduction

[2] The discovery of coesite eclogites in some orogens deeply modified geodynamic concepts on continental geodynamics. It is now widely acknowledged that continental crust can be subducted to depth larger than 100 km (i.e., into the asthenosphere). However, tectonic studies of UHP belts are still rare. In China, the Qinling Belt results of the collision between the North China Block (NCB) and the South China Block (SCB) [e.g., *Mattauer et al.*, 1985, 1991; *Okay et al.*, 1993]. The Dabieshan massif that forms the eastern part of the Qinling Belt is one of the largest areas in the world where ultrahigh-pressure (UHP) metamorphic rocks are widespread. To the east of the Dabieshan, the Qinling Belt is abruptly interrupted by the NNE-SSW trending Tan-Lu fault, but similar rocks crop out 500 km northward in the southern part of the Shandong Peninsula or Sulu area (Figure 1). Alike the Dabieshan, the Sulu area is a famous place for UHP metamorphism [e.g., *Enami and Zhang*, 1990; *Enami et al.*, 1993a; *Hirajima et al.*, 1990; *Zhang et al.*, 1994, 1995; *Cong*, 1996], but structural studies are still limited [*Wallis et al.*, 1997, 1999]. It is generally accepted that the boundary between NCB and SCB lies in the central part of the Shandong peninsula, but recently on the basis of structural and petrologic evidence, it has been argued that the whole Shandong Peninsula belongs also to the SCB [*Faure et al.*, 2001]. This paper aims to present new field structural data and kinematic analyses on the ductile synmetamorphic structures of Shandong peninsula. New petrological and $^{40}Ar/^{39}Ar$ dates are also used to discuss a possible geodynamic evolution of the Qinling Belt east of the Tan-Lu fault.

2. Geological Outline of the Shandong Peninsula

[3] East of the Tan-Lu fault, the Shandong Peninsula consists of several units (Figure 2). The southern part of the peninsula where UHP rocks crop out is called Sulu area, whereas the northern part consists of "Jiaodong gneiss." Classically, the former belongs to the SCB and the latter to the NCB [e.g., *Cong*, 1996]. However, in the following, we

[1]Institut des Sciences de la Terre d'Orléans, UMR 6113, Université d'Orléans, Orléans, France.
[2]Institute of Geology and Geophysics, Chinese Academy of Sciences, Beijing, China.
[3]Laboratoire de Géophysique, Tectonique et Sédimentologie, Université des Sciences et Techniques du Languedoc, Montpellier, France.
[4]Centre de Recherches Petrographiques et Geochiminique and Centre National de la Recherche Scientifique (CRPG-CNRS), Vandoeuvre-les-Nancy, France.

0278-7407/03/2002TC001450$12.00

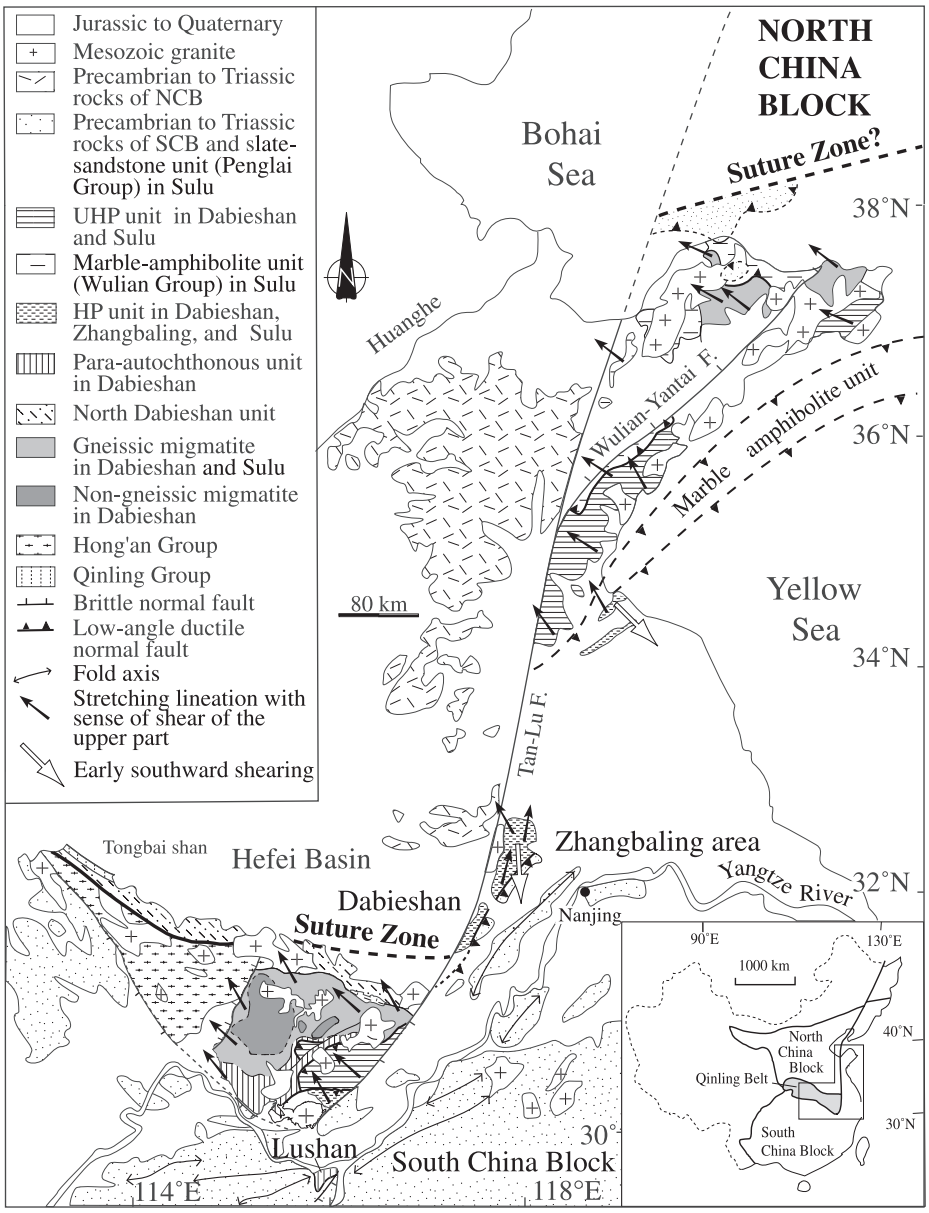

Figure 1. Correlation map of structures between Dabieshan and Sulu area.

shall argue that these two domains belong to the SCB. The central part of the Shandong Peninsula is a NNE-SSW trending Cretaceous sedimentary basin with red continental sandstone and volcanic layers overlying early Cretaceous granitoids and metamorphic rocks.

2.1. Sulu Area

[4] The Sulu area is a stack of tectonometamorphic units (Figures 1 and 2). The southern and uppermost unit, well exposed along the seacoast near Lianyungang is formed by ortho- and paragneiss, and volcanic-sedimentary rocks (called the Haizhou group [*Shandong Bureau of Geology and Mineral Resources* (*SBGMR*), 1991]). These rocks experienced a high-pressure (HP) metamorphism [*Cong*, 1996]. The Haizhou-Siyang fault inferred by geophysics separates the southern HP Unit from the northern UHP one. Lithologically, the UHP Unit is similar to the HP one. It consists of orthogneiss, paragneiss, quartzites, marbles and meter to hectometer sized blocks of mafic rocks, ultramafic rocks also crop out. Due to the discovery of jadeite in orthogneiss near Qingdao [*Hirajima et al.*, 1993] and coesite in marble [*Kato et al.*, 1997] it is now well acknowledged that the UHP metamorphism affected a coherent slab of continental crust. The coesite eclogites are not oceanic blocks tectonically inserted in continental rocks but correspond to basalt or dolerite dykes, gabbros and pyroxenitic cumulates that intruded the continental crust and underwent continental subduction and subsequent UHP metamorphism together with their host rocks [*Zhang et al.*, 1994, 1995, 2000; *Yang et al.*, 1993; *Jahn*,

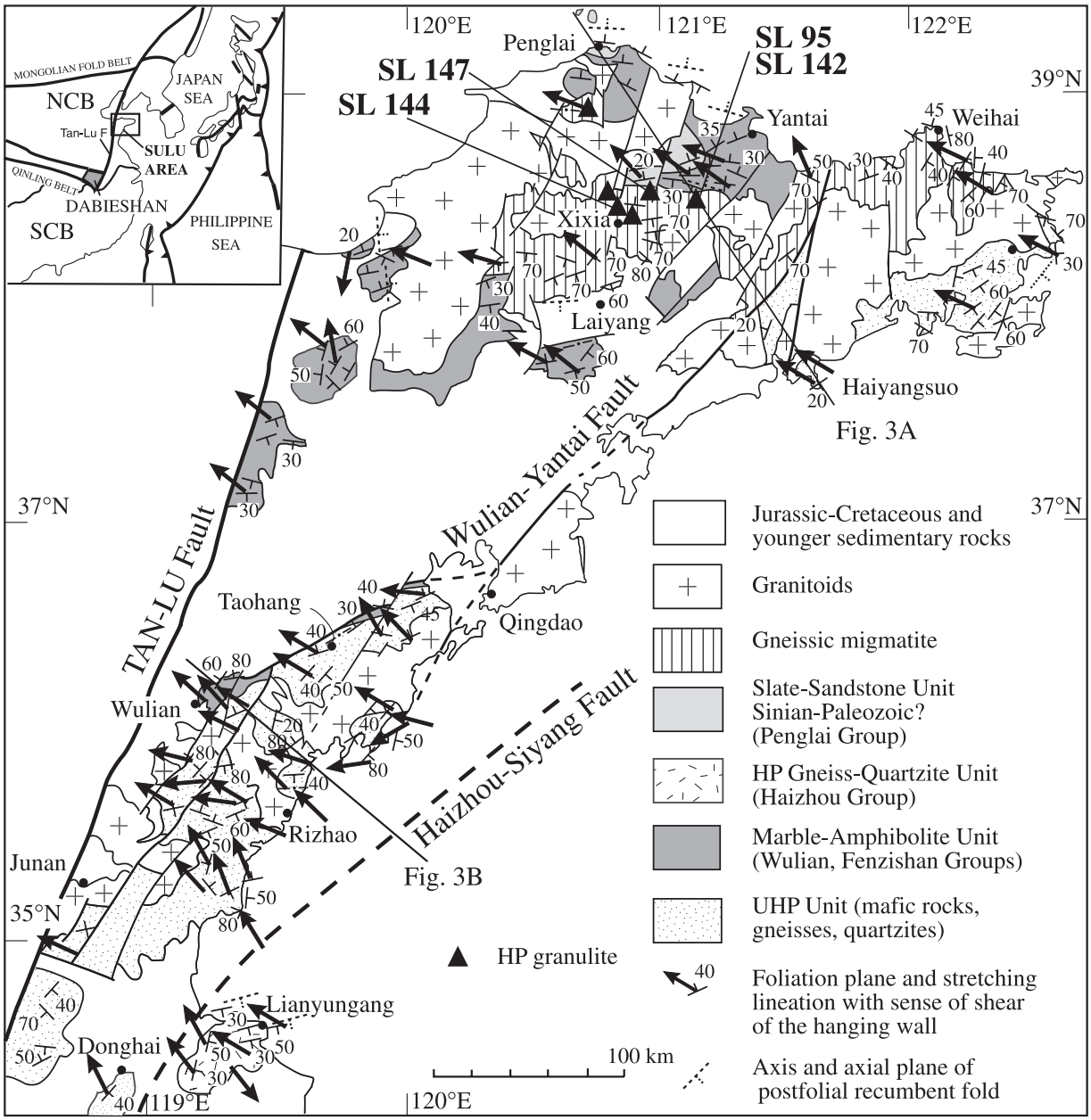

Figure 2. Structural map of the Shandong peninsula. Numbers SL 95, SL 142, SL 144, SL 147 correspond to the granulites analyzed in section 4. Note the top-to-the-SE shearing limited to Lianyungang area. (Modified from *Faure et al.* [2001].)

1999; *Yang and Jahn*, 2000]. Between Junan and Qingdao, the foliation of the UHP Unit is folded by a NE-SW trending antiform, north of which a Marble-Amphibolite Unit (called the Wulian Group) crops out. The Marble–Amphibolite Unit is devoid of any UHP mineral and it tectonically overlies the UHP Unit. A 800 m thick mylonitic-ultramylonitic shear zone separates both units (Figures 3, 4c, and 4d).

2.2. North Shandong Area

[5] North of the Cretaceous basin, three metamorphic units crop out, namely from top to bottom: (1) the Slate-Sandstone Unit, (2) the Marble-Amphibolite Unit, and (3) the Laiyang migmatitic dome (Figure 1).

[6] The Slate-Sandstone Unit consists of weakly metamorphosed terrigenous rocks called the Penglai Group [*SBGMR*, 1991]. These rocks are generally assigned to Neoproterozoic (Sinian) but an Early Paleozoic age is also suggested on the basis of poorly preserved bivalves [*Ji and Zhao*, 1992; *Cong*, 1996]. The Slate-Sandstone Unit is mapped as unconformably covering the Marble-Amphibolite Unit; however, as shown below, this contact is tectonic and refolded during the second deformation event (cf. section 3.3).

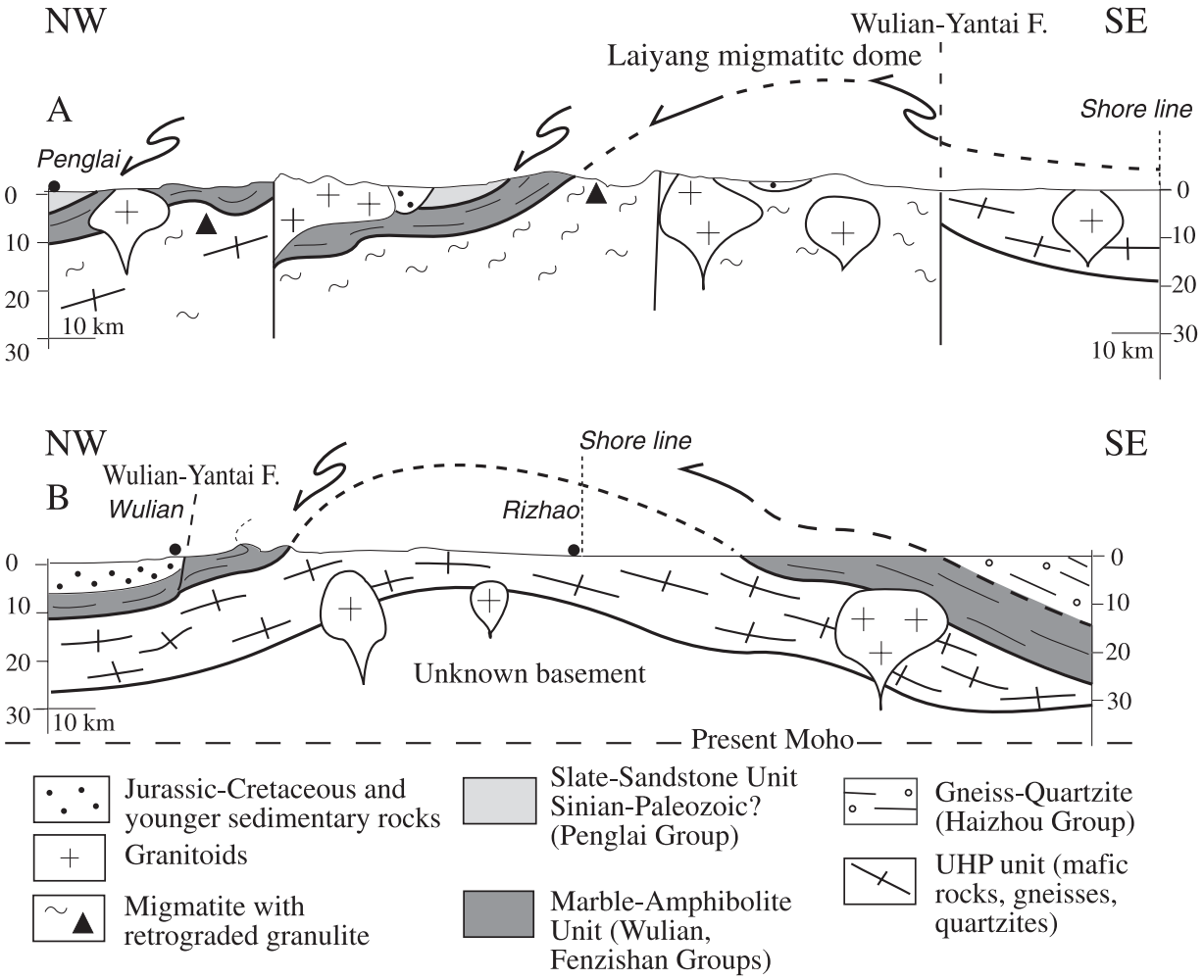

Figure 3. Schematic cross sections through the Shandong Peninsula (located in Figure 2). (Modified from *Faure et al.* [2001].)

[7] In Northern Shandong, marble, micaschist and amphibolite (diabase, sills and dykes) underlying the Slate-Sandstone Unit are called the Fengzishan Group [*SBGMR*, 1991]. However, from lithological, metamorphic and structural points of view, there is no significant difference between these rocks and those of the Wulian Group in the Sulu area. Therefore these rocks are grouped here into a single lithologic-tectonic unit, the Marble-Amphibolite Unit which underlies the Cretaceous basin of central Shandong (Figure 3).

[8] The main part of North Shandong is formed by a well foliated diatexite, but locally well preserved nebulitic structures with contorted leucosomes and K-feldspar porphyroblasts show that those gneiss experienced partial melting before their deformation. It is worth to note that meter to hectometer large blocks of mafic rocks are found in the migmatite. These rocks are considered as restites that, due to their Fe-Mg rich chemical composition did not experience melting when Al-Si rich rocks underwent migmatization. Most of these rocks are amphibolites formed by retrogression of earlier granulitic and eclogitic assemblages [e.g., *Zhai et al.*, 2000; *Faure et al.*, 2001]. These rocks are very important to discuss the geodynamic significance of the North Shandong area with respect to the UHP rocks of the Sulu area. Their petrology will be presented in detail in section 4.

2.3. Weihai Migmatite

[9] In East Shandong, around Weihai (Figure 2), migmatites are also widely exposed. These rocks contain retrogressed HP-granulites and in a few places coesite and omphacite inclusions in garnet demonstrate that these rocks experienced the UHP metamorphism [*Wang et al.*, 1993]. For this reason, it is well accepted that the Weihai migmatite belongs to the Sulu area and consequently, to the SCB. However, the petrologic and structural resemblances between the Weihai and North Shandong migmatites lead us to consider that these two units belong to the same one (cf. discussion in section 6).

[10] The bulk geometry of Shandong Peninsula corresponds to a central synform filled by Cretaceous sedimentary rocks flanked by two antiforms where granite and metamorphic rocks are exposed (Figure 3). This regional scaled structure is obviously a Cenozoic one that reworks

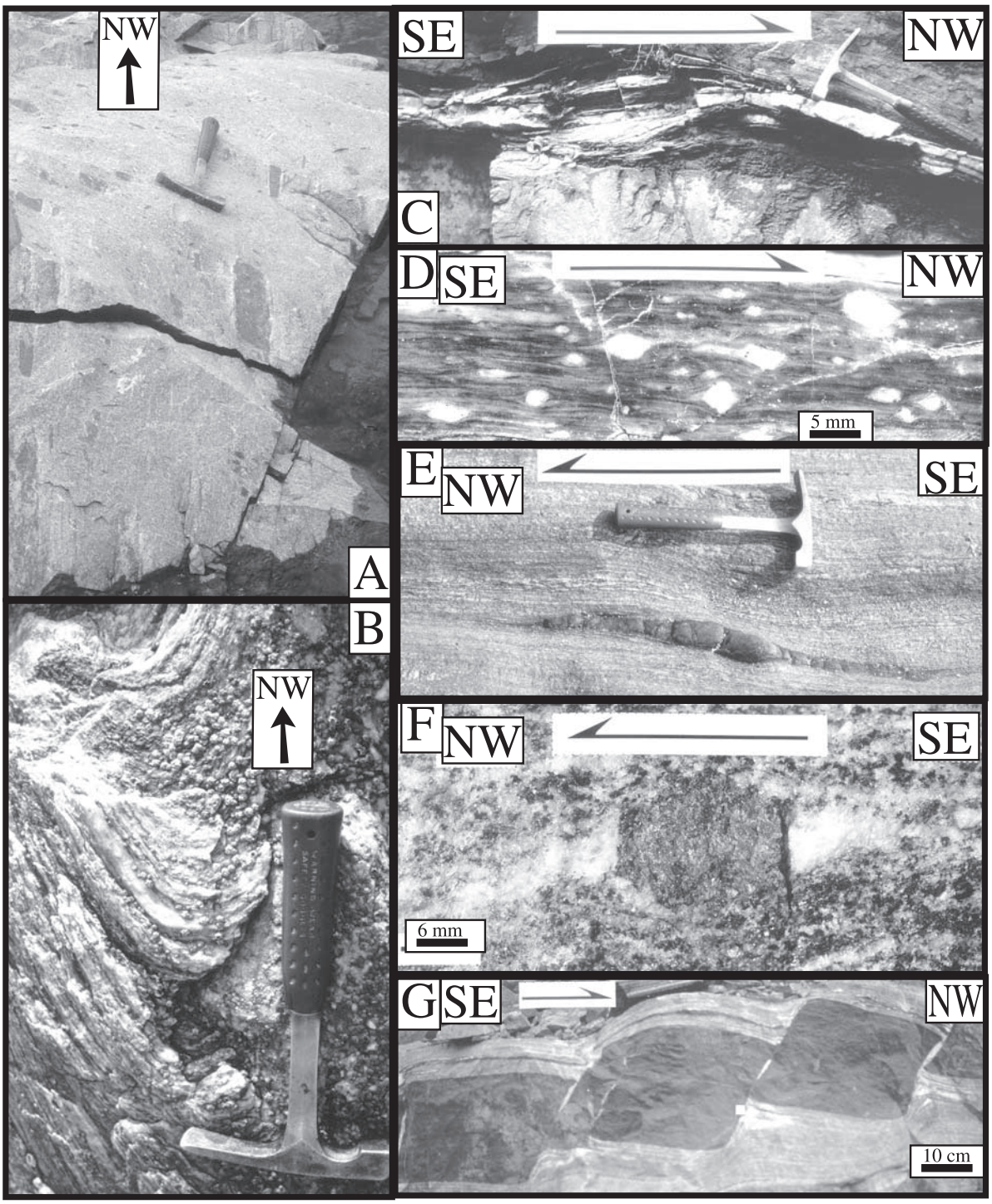

Figure 4. A: Orthogneiss with NW-SE stretched enclaves, HP gneiss-quartzite Unit, South of Lianyungang. B: Sheath fold in leucocratic gneiss hosting eclogite, arrow is parallel to the regional stretching lineation, Haiyangsuo. C: Sigmoidal mylonitized quartz vein in the UHP Unit close to its upper tectonic boundary with the Marble-Amphibolite Unit, South of Wulian. D: Ultramylonite showing top-to-the-NW sigma- and delta-type porphyroclast systems in the UHP Unit close to its upper tectonic boundary with the marble-amphibolite Unit, South of Wulian. E: Sigmoidal mafic lenses (probably enclave) in mylonitic orthogneiss showing a top-to-the-NW sense of shear. F: Asymmetric quartz pressure shadows around garnet indicating top-to-the-NW sense of shear in gneissic migmatite enclosing granulitic block, Xixia. G: Rotated amphibolite boudins showing top-to-the-NW shearing in gneissic migmatite near Xixia.

older synmetamorphic structures. The polyphase deformation, kinematics and timing of the ductile structures are analyzed in the next section.

3. Polyphase Deformation of the Shandong Peninsula

[11] Our field survey in the Shandong Peninsula allows us to decipher several tectono-metamorphic events that shaped up this domain. We shall successively examine the Sulu and North Shandong areas.

3.1. Main Deformation in the Sulu Area

[12] Except for the Cretaceous granite, whatever the protolith or metamorphic grade, the whole Sulu area consists of foliated and lineated rocks. A NW-SE trending mineral and stretching lineation is the most significant microstructure of the Sulu area (Figure 4a). It is worth noting that in spite of local perturbations (E-W or N50°E directions), this lineation develops in all kinds of lithology and whatever the metamorphic grade. Indeed, this lineation developed under amphibolite facies conditions. Along the contact between the UHP and overlying Marble-Amphibolite Units, the gneissic foliation evolves toward mylonitic and ultramylonitic fabrics (Figures 4c and 4d). In the quartzo-feldspathic rocks, the mineral lineation is marked by elongated quartz rods or feldspar aggregates. In the carbonates, calcite or dolomite grains are often recrystallized. In the marbles or mafic rocks of the Marble-Amphibolite Unit, the lineation is defined by stretching or oriented crystallization of calcite, dolomite, tremolite, olivine, hornblende and epidote.

[13] Classical shear criteria such as such as σ- or δ-type porphyroclast systems, quartz or calcite pressure shadows provide a consistent top-to-the-NW sense of shear (Figures 4c, 4d, 5d, and 7d). Similar top-to-the-NW shearing is observed in every type of rock. Small mafic lenses exhibit sigmoidal shapes (Figure 4e). In highly sheared zones, such as mylonitic contact or along lithological interfaces (for instance between metabasite and gneiss) sheath folds develop (Figure 4b). Lattice preferred orientation (LPO) of quartz has been measured using an X-ray texture goniometer. The ⟨1014⟩ and ⟨1120⟩ quartz subfabrics which are close to ⟨c⟩ and ⟨a⟩ axes respectively confirm the kinematics inferred from macroscopic and microscopic shear criteria (Figure 5). Moreover, the subfabric diagrams provide useful information on the deformation conditions. As shown by the ⟨c⟩ axis maxima near the diagram center (SL 118) or close to the foliation pole (SL 38, SL 72) the basal ⟨a⟩ and prism ⟨a⟩ were the active slip systems. Such features comply with moderate deformation temperature conditions (∼350°–400°C) or high strain rates ($\sim 10^{-18}$–10^{-20}% s^{-1}) together with significant water content [e.g., *Law*, 1990].

[14] As shown by cracked garnet and boudinaged omphacite, the eclogite facies minerals deform after their crystallization. All the above described kinematic markers develop coeval with the amphibolite facies associated to the retrogression of the UHP assemblages. Thus, these microstructures cannot be used to discuss the deformation pattern associated to continental subduction but bring information on the tectonics responsible for the exhumation of the UHP Unit.

[15] However, in a few gneiss exposures found in the southern HP Gneiss-Quartzite Unit (sample SL 38) near Lianyungang (Figure 2), top-to-the-SE shearing is observed both in the field and in thin section from shear criteria and quartz LPO (Figure 5). These structures are interpreted as rare relicts of the early compressional stage that preceded the synkinematic top-to-the-NW retrogression. Similar features, which are also found more to the south in the Zhangbaling area or in the Dabieshan (Figure 1), will be discussed in section 6.

3.2. Laiyang Migmatitic Dome of North Shandong

[16] In spite of local perturbations of the regional foliation by NE-SW trending faults, the variations of the foliation trend throughout the migmatitic domain of N. Shandong support a domal structure for these rocks. This structural arrangement is strengthened if the eastward dipping migmatite cropping out between Yantai and Weihai are also attributed to the same dome. Conversely to the changing geometry of the foliation, the mineral and stretching lineation keeps a constant NW-SE trend throughout the migmatitic dome. A remarkable exception can be found at the western end (west of Laiyang, Figure 2) where the lineation trend turns to NE-SW. This feature is explained by foliation refolding due to the second deformation phase (cf. below in section 3.4).

[17] The migmatitic structures such as concentrations of mafic minerals, folded leucosomes, nebulitic layers are locally preserved, but in general, the migmatite appears as a well banded and lineated gneiss with intrafolial folds (Figure 6b). Quartz, feldspar, and amphibole recrystallization textures show that these planar and linear microstructures were acquired under post-solidus conditions, i.e., after crystallization of the melt. On the upper part of the Migmatitic Unit, close to its contact with the Marble-Amphibolite Unit, west of Yantai, the foliated migmatite is transformed into mylonite or ultramylonite. Alike for the Sulu area, shear criteria such as σ- or δ-type porphyroclast systems, rotated boudins, quartz pressure shadows around garnet, sigmoidal micas, etc., indicate a top-to-the-NW shearing (Figures 2, 4f, 4g, and 7c). This kinematic pattern is in agreement with quartz L P O. Some of the most representative subfabrics of quartz ⟨a⟩ and ⟨1104⟩ axes are given in Figure 5. The diagram asymmetries are in agreement with the top-to-the-NW shearing. In addition, the ⟨1104⟩ axis maximum, close to the center of the diagram (i.e., perpendicular to the lineation), indicates that ⟨a⟩ prism was also an activated slip system. Therefore the main ductile deformation of the North Shandong migmatitic dome occurred under medium temperature (∼350°–450°C) or slow strain rate (10^{-18}–10^{-20}% s^{-1}), that is to say, under transition of greenschist to amphibolite facies conditions.

3.3. Deformation of the Marble-Amphibolite and Slate-Sandstone Units

[18] Alike the migmatitic gneiss, the Marble Amphibolite Unit (Fengzishan Group) that surrounds the migmatitic dome is also deformed by two ductile events. The second

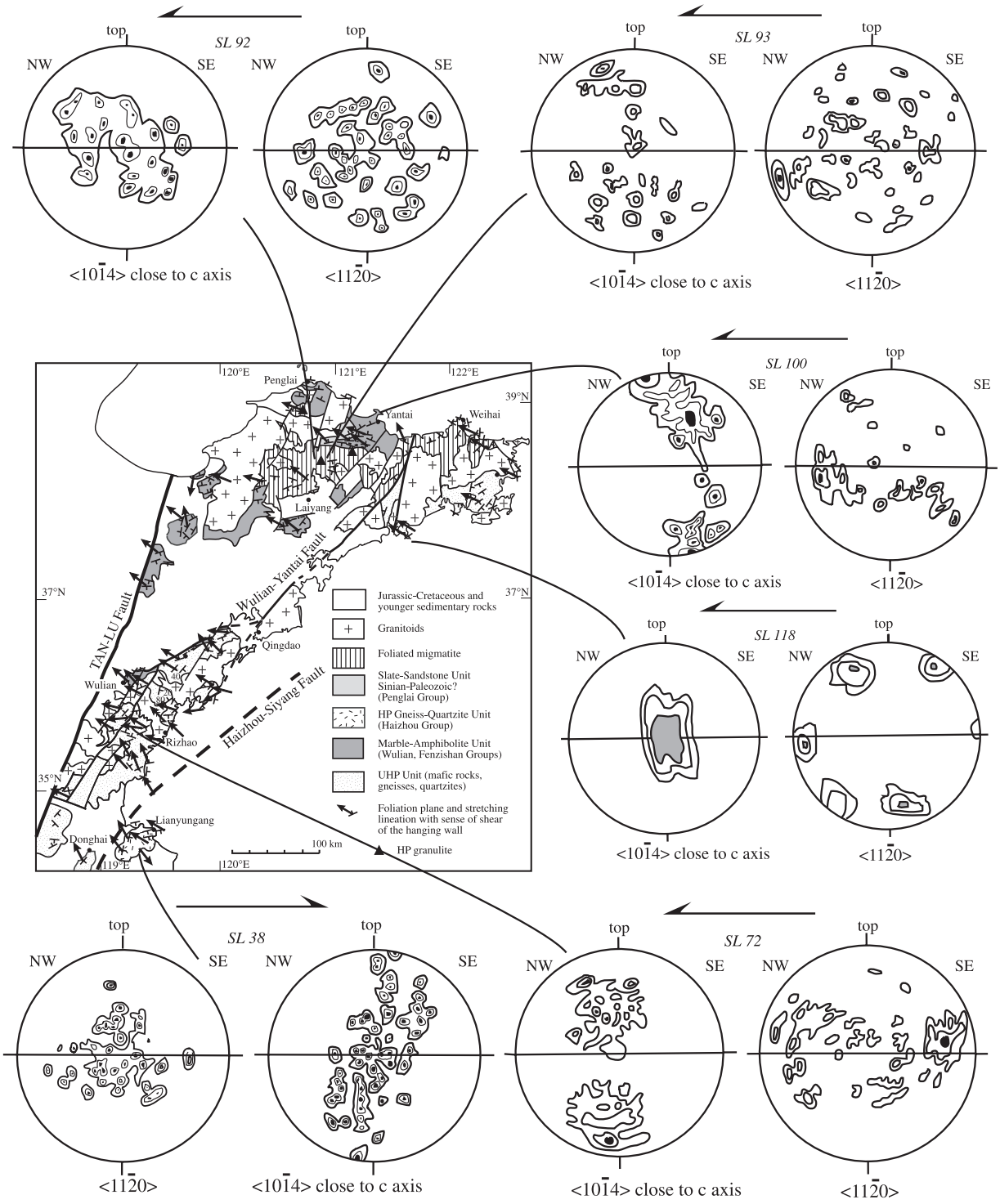

Figure 5. Examples of quartz lattice preferred orientation obtained by texture goniometry. Note that except for an orthogneiss in the HP gneiss-quartzite Unit (sample SL 38) showing top-to-the-SE sense of shear, other rocks consistently indicate top-to-the-NW shearing. Samples are quartz rich gneiss from UHP Unit (SL 118), ultramylonite (SL 72), gneissic migmatite (SL 92, 93) and marble-amphibolite Unit (SL 100). All diagrams are lower hemisphere Schmidt net drawn in the XZ section of the bulk strain ellipsoid (i.e., perpendicular to foliation and parallel to lineation). Contour intervals are 1.5%, 3%, and maximum 5% multiple of random distribution for samples SL 93, SL 100, SL 118 and SL 72; and 1.5%, 2% and maximum 3% for samples SL 92 and SL 38.

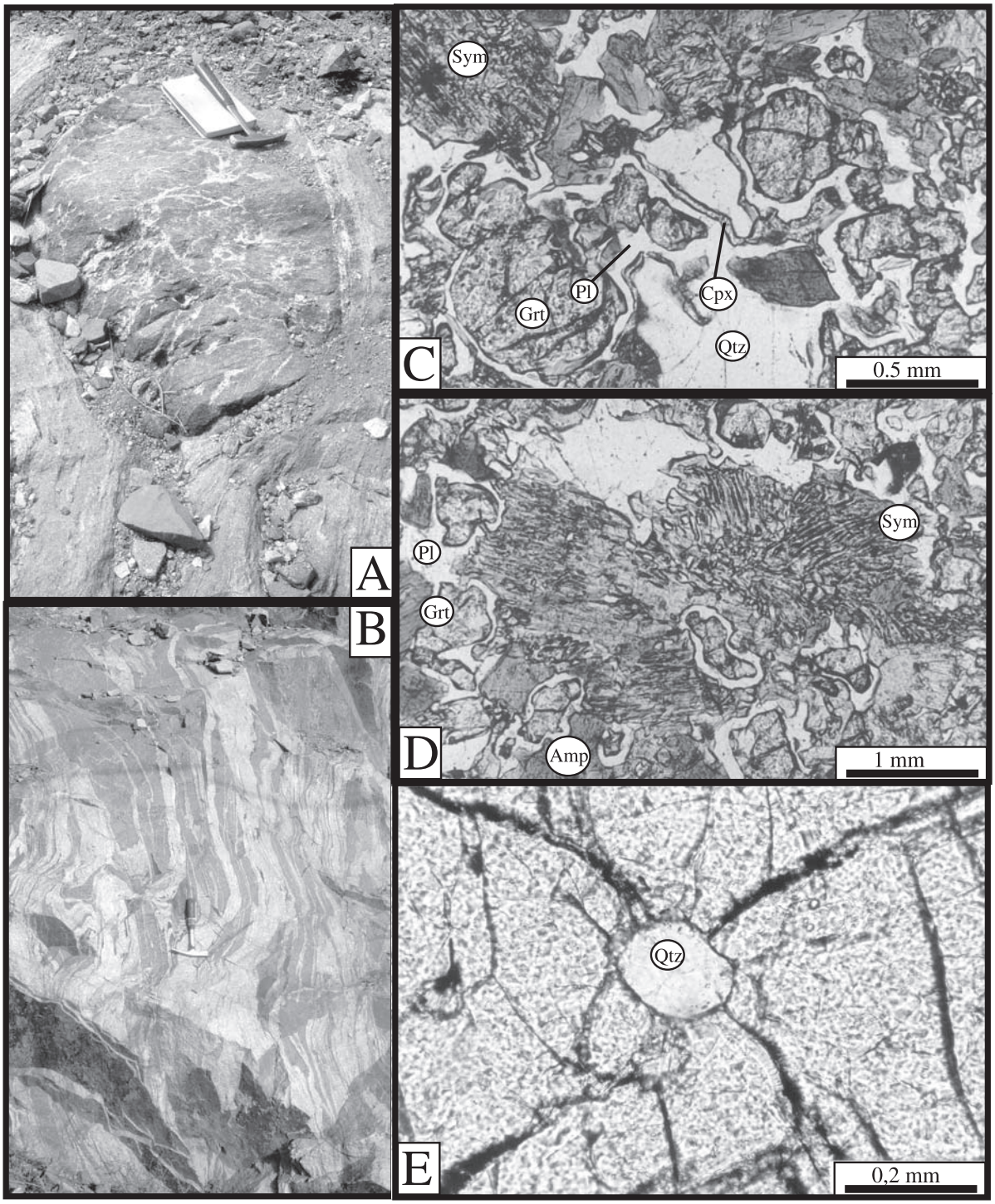

Figure 6. A: Field occurrence of granulite boudin enclosed in a well-foliated migmatite. Note the migmatitic melt veins that invade the metabasite. Due to high strength of the boudin, these leucosomes are preserved from deformation. B: Typical aspect of the N. Shandong migmatite. C: Microphotograph of the North Shandong granulite (Sample SL 95 located in Figure 2) showing coronitic relation between garnet, plagioclase and clinopyroxene (Qtz, Grt, Pl, Amp, Cpx, Sym for quartz, garnet, plagioclase, amphibole, clinopyroxene and clinopyroxene-plagioclase symplectite respectively). D: Microphotograph of the North Shandong granulite showing garnet surrounded by plagioclase, and clinopyroxene-plagioclase symplectite probably formed at the expense of omphacite (see text for discussion). Captions are the same as in Figure 6c. Sample SL 95 is located in Figure 2. E: Quartz inclusion surrounded by radial cracks in garnet suggesting that it might be the result of the polymorphic transition from coesite to quartz.

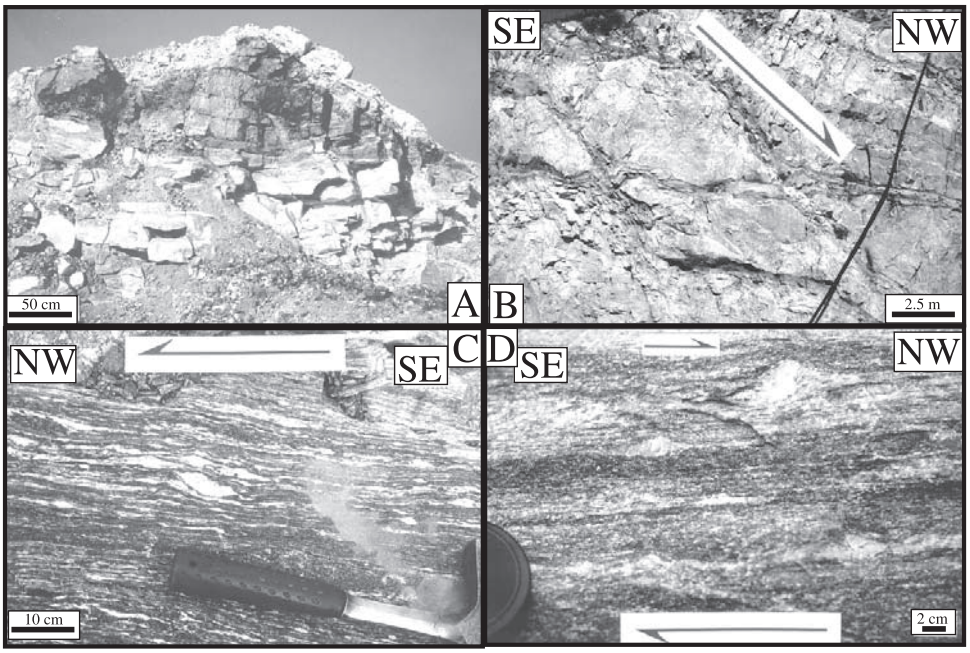

Figure 7. A: Metabasite boudin in the Marble-Amphibolite Unit South of Laiyang. B: High angle brittle normal fault in the Marble-Amphibolite Unit South of Yantai. C: Mylonitic migmatite showing top-to-the-NW sheared quartzo-feldspathic veins, South of Penglai. D: Ultramylonite with top-to-the-NW sigma-type porphyroclast, basal shear zone at the contact with the Marble-Amphibolite Unit, NW of Rizhao.

event which is responsible for the domal structure will be described below in section 3.4. When not strongly disturbed by this second event, structures related to the first one exhibit similar features. For instance, centimeter to decameter scale boudinaged mafic dykes enclosed in marble show a top-to-the-NW shearing in agreement with the kinematics in the migmatite (Figure 7a).

[19] In the weakly metamorphosed Slate-Sandstone Unit, the lineation is poorly marked, but slickenlines with the same direction are observed on bedding planes. Moreover, near the basal contact with the Slate-Sandstone Unit, in the Marble-Amphibolite Unit, tremolite-bearing asymmetric marble boudins are deformed by ductile normal faults the hanging wall moving northward (Figure 7b); and in the Slate-Sandstone Unit, folds overturned to the NW develop. These structures suggest that the initial stratigraphic boundary between the Slate-Sandstone Unit and underneath units, which might have been initially an unconformity, have been reworked as a northwest directed detachment fault during the main tectonic event.

[20] Conversely to the Sulu area, it is worth to note that in the present state of knowledge, top-to-the-south shearing, likely be related to an earlier compressional event, is not observed in the North Shandong area. The kinematic picture of the early ductile deformation in the whole Shandong Peninsula is presented in Figure 2.

3.4. Polyphase Deformation in North Shandong Area

[21] At the western end of the Laiyang dome, the lineation trends NE-SW (N20°E to N50°E) and exhibits a top-to-the-SW shear sense (Figure 2). This abnormal kinematic pattern can be explained by a polyphase deformation. The primary foliation and NW-SE lineation are folded by N-S trending F2 folds. During this deformation, the early kinematic criteria are changed from NW to SW sense of shear (Figure 8). This second ductile deformation which refolds the foliation, lineation and intrafolial folds is observed in

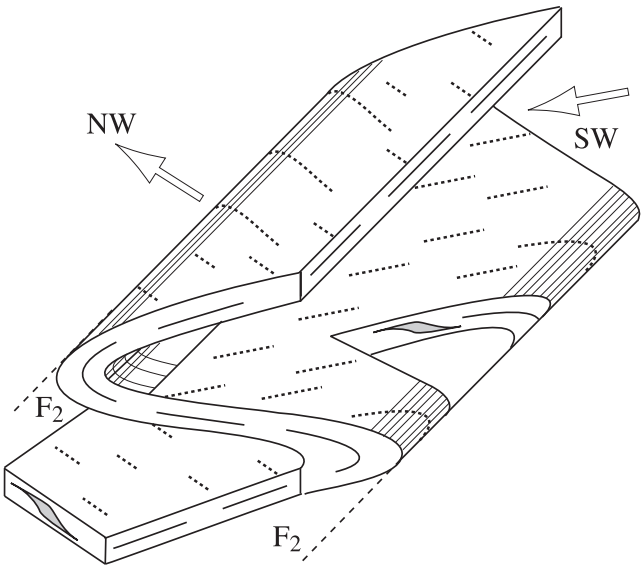

Figure 8. Interpretative diagram showing how secondary (F2) folding of the foliation and lineation may produce locally apparent top-to-the-SW shearing.

several places all around the Laiyang dome. Along the sea coast, SE of Weihai, isoclinally folded and top-to-the-NW sheared gneiss are deformed by N10°E to N40°E trending folds overturned to the SE. Along the northern margin of the dome, from Penglai to Yantai, the early fabric (foliation, lineation and intrafolial folds) is locally turned to the vertical or even dips to the SW. On the western side of the dome, the foliation is turned to vertical by N-S trending folds overturned to the west. As a matter of fact, these second phase structures indicate a divergent pattern. The folds deforming the foliation are consistently overturned to the west, northeast, southeast and south on the west, north, southeast and south sides of the dome, respectively. The subhorizontal axial planes of these secondary folds indicate a bulk subvertical shortening that supports an extensional tectonic setting for this post-folial deformation phase.

4. Petrology of the HP Granulite Restite in the Laiyang Migmatitic Dome

[22] The migmatite of the Laiyang dome contains numerous meter- to decameter-size mafic restites exposed either as blocks wrapped in the foliation or as continuous layers parallel to the foliated migmatite (Figures 6a and 6b). Most of these metabasites are amphibolites but granulitic assemblages are also reported [e.g., *Zhai et al.*, 2000; *Faure et al.*, 2001].

4.1. Mineralogical and Textural Description

[23] In the studied mafic samples, located in Figure 2, garnet, clinopyroxene, amphibole, quartz and plagioclase are the principal minerals. Minor phases such as orthopyroxene, zircon, apatite and opaque are also present. Several metamorphic textures such as vermicular symplectites and coronites show that all these minerals did not crystallize at the same time.

[24] The garnets are systematically anhedral. In some samples (SL95), garnets are isolated from the green amphibole and/or from the clinopyroxene by a single corona of plagioclase (Figure 6d) whereas a double corona has crystallized between garnet and quartz. In this latest case, the plagioclase is always in contact with garnet whereas the clinopyroxene forms thin stripes around quartz grains (Figure 6c). In other samples (SL142, SL147), garnets are surrounded by symplectites made of green amphibole and of a very fine mixture of white micas and zoisite. Another very common symplectite is made of two minerals, clinopyroxene and plagioclase (Figure 6d). The clinopyroxene forms about 60% (volume) of the symplectite and it includes blobs of plagioclase. These vermicular two-phase associations show external forms that could be those of previous clinopyroxene grains.

[25] Amphibole is always present as large crystals. Sometimes small grains of a green amphibole are also associated together with plagioclase in symplectitic coronas around garnets. It is worth to emphasize that plagioclase is never present as (sub)euhedral grains but it forms very often thin ribbons surrounding either garnet or clinopyroxene (Figures 6c and 6d). Sometimes, it appears as large poikiloblastic crystals including grains of garnet, clinopyroxene, amphibole and quartz and separating them one from another. Otherwise, plagioclase is associated with clinopyroxene (Figure 6d) or with amphibole in symplectites. Quartz is not a rare mineral in these mafic rocks and some samples have been selected for coesite investigations. In one sample (SL95), a thin section shows circular inclusions in a garnet that is affected by radial cracks (Figure 7e). Unfortunately the RAMAN investigation reveals only quartz in these inclusions. Nevertheless, the presence of quartz does not preclude that these inclusions were initially coesite. The temperature increase during migmatization might have been high enough to induce a phase transition from coesite into quartz. The question of the preservation of UHP rocks after the exhumation of the subducted continental crust will be discussed and compared with the Dabieshan in section 6.

4.2. Mineral Compositions

[26] The four major phases (garnet, clinopyroxene, plagioclase and amphibole) have been analyzed using a Cameca electron microprobe (BRGM-CNRS-University in Orléans, France). Only a few plots are given here (Figures 9, 10, and 11). Depending on the sample, the garnet contains generally 40 to 60 mole% of almandine, 10 to 30 mole% of pyrope and 20 to 40 mole% of grossular. The zonations detected in chemical profiles are generally limited to a slight increase in iron and a slight decrease in magnesium at the outermost rim, and the cores of the grains appear as rather homogeneous.

[27] All analyzed clinopyroxene have compositions ranging between diopside and augite (Figure 10). Their content in jadeite end-member is negligible. They do not show any noticeable zoning. Plagioclase exhibits generally a quite heterogeneous composition. For example, in the sample SL 95 (Figure 11), the anorthite content of the mineral increases in the coronas from the rim in contact with clinopyroxene to the rim in contact with garnet. It is very difficult to analyze the very small plagioclase blobs associated with calcic clinopyroxene in the symplectites but maps of sodium and calcium distribution seem to show similarities with the plagioclase composition of the outer coronas. The large crystals of amphibole observed in the different samples are rather homogeneous and they have essentially a composition of tschermakite. The small grains found in the coronas surrounding some garnets are magnesiohornblendes (according to the nomenclature proposed by *Leake et al.* [1997]).

4.3. Textural Interpretation

[28] The textures described above can be interpreted in terms of mineralogical reactions. First, the symplectitic associations of calcic clinopyroxene and plagioclase are probably the breakdown products of eclogitic omphacite crystals as the pressure decreases from the eclogite facies conditions to the granulite facies ones. Preliminary mass balance calculations show that if the supposed initial omphacite had a Na_2O-content of 7 to 8 wt % as in the eclogites sampled in the Sulu area [*Yao et al.*, 2000], and if it was completely replaced by the symplectite during the decompression, this association would have to form 25 wt % of the rock SL95. This content is in good agreement with the value

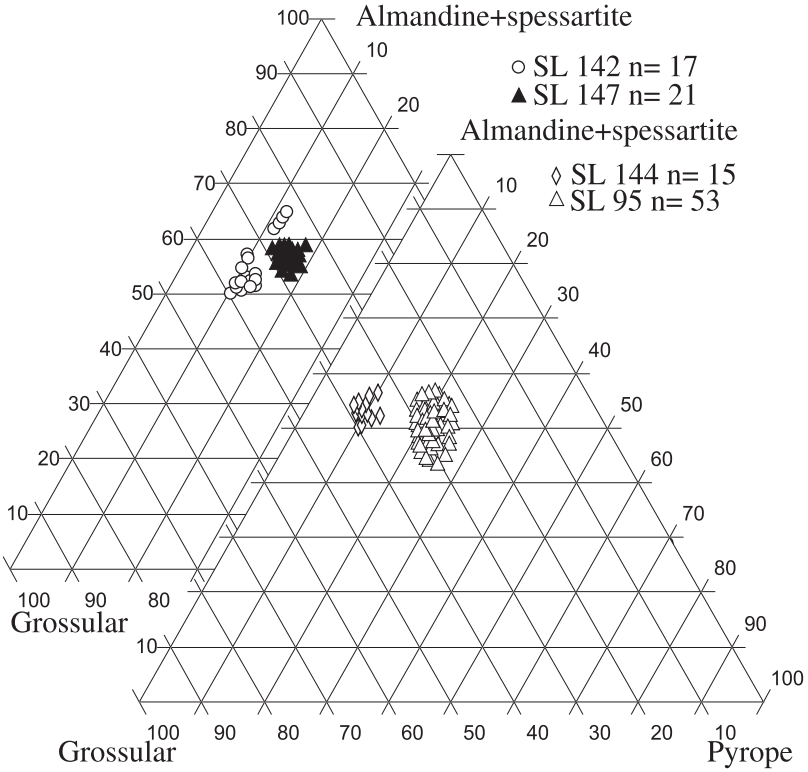

Figure 9. Chemical analysis of garnet from the North Shandong granulites, sample location in Figure 2.

really found in the sample (about 23 wt %). Thus, the presence of omphacite in the rock in an earlier eclogitic stage is quite possible.

[29] Second, it is worth to note that plagioclase crystallized exclusively as a secondary phase. The plagioclase coronas surrounding those garnets that are isolated from amphibole by the feldspar suggest, although nonequilibrated, the following dehydration reaction: garnet + tschermakite → plagioclase + H_2O. Conversely, the double coronas of plagioclase and clinopyroxene separating garnet from quartz can be interpreted as the result of a reaction such as: garnet + quartz → plagioclase + Ca-clinopyroxene. In this case, the relative immobility of aluminum during the reaction is suggested by the presence of the aluminum-richer

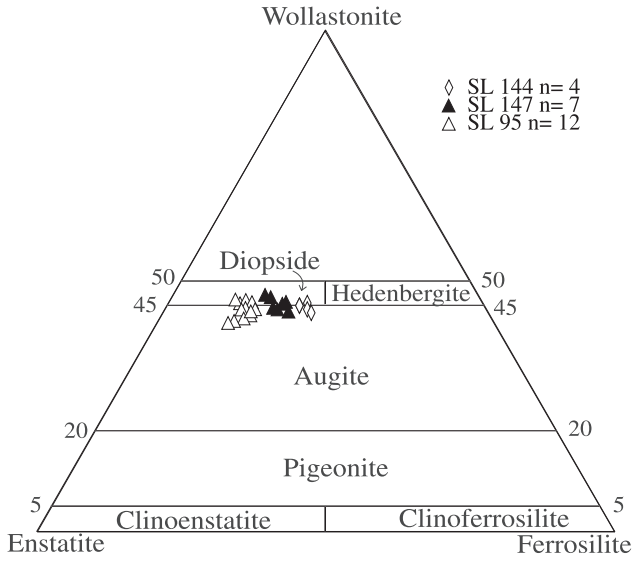

Figure 10. Chemical analysis of clinopyroxene from several granulite blocks in the N. Shandong migmatitic dome, sample location in Figure 2.

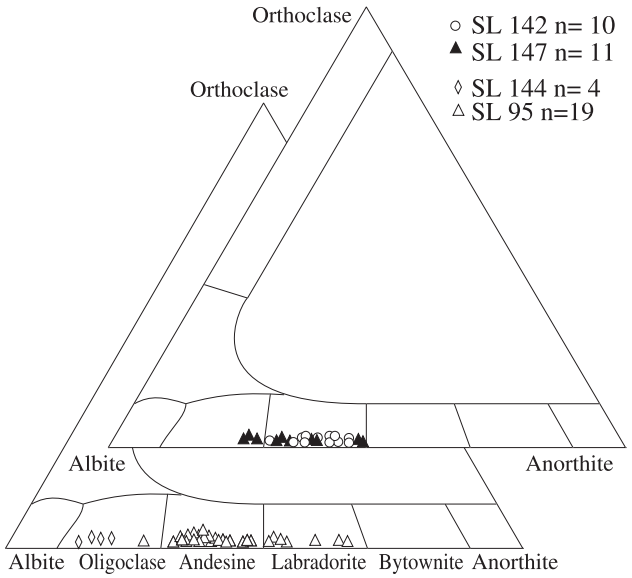

Figure 11. Chemical analysis of plagioclase from granulite blocks in the N. Shandong migmatitc dome.

product (i.e., plagioclase) in contact with the aluminum-richer reactant (i.e., garnet); the aluminum-poorer product (clinopyroxene) being present in contact with quartz. Both reactions may transform a plagioclase-free eclogitic paragenesis into a plagioclase-bearing granulitic assemblage.

[30] Third, the presence of coronas composed of magnesiohornblende and plagioclase (more or less transformed into white mica and zoisite) around some garnets can be interpreted as the result of the hydration reaction: garnet + clinopyroxene + $H_2O \rightarrow$ magnesiohornblende + plagioclase. This reaction is classically explained by a decrease of pressure and temperature in presence of water that transforms an eclogitic or granulitic paragenesis into an amphibolitic assemblage.

[31] The interpretation of the different textures suggests therefore the following evolution of the mafic assemblages: an eclogitic paragenesis (garnet + omphacite + tschermakite + quartz) was transformed into a plagioclase-bearing granulitic assemblage including the presence of a calcic clinopyroxene before a part of the garnet has reacted together with clinopyroxene and water to form magnesiohornblende and plagioclase. The first stage in the eclogite facies conditions would have been followed by a decompression phase (total breakdown of omphacite) and a heating phase (partial breakdown of tschermakite) bringing the paragenesis into the granulite facies before the final retrogression leads to the partial breakdown of the previous mineral assemblages in the amphibolite facies conditions.

4.4. Thermobarometry

[32] The samples SL95 and SL147 allow combining the classical thermometer using the iron-magnesium exchange between garnet and clinopyroxene [*Ellis and Green*, 1979; *Krogh*, 1988; *Pattison and Newton*, 1989] and the barometer based upon the equilibrium: plagioclase + clinopyroxene $\Longleftrightarrow$ garnet + quartz [*Newton and Perkins*, 1982]. If the above discussed textural interpretation is correct, it can be expected that the pressure-temperature (P-T) conditions computed by combining these thermometer and barometer correspond to granulitic conditions. It is in fact the case since the calculations taking into account the works of *Moescher et al.* [1988] and of *Perkins* [1990] yield the following results: $750° \pm 40°C$ and 12.9 ± 1.6 kbar, and $810° \pm 40°C$ and 13.1 ± 1.6 kbar for SL95 and SL147, respectively.

[33] These preliminary results have to be confirmed by a very thorough work on textures and phase compositions. However, it is already obvious that thermobarometry of these samples does not allow us to estimate the probable early eclogitic conditions since no more omphacite is present in the restitic metabasites. It is however remarkable that the conditions determined here are those of high-pressure granulites, at the boundary with true eclogitic conditions.

4.5. P-T Path

[34] The granulite facies P-T conditions of ca 800°C-13 kbar derived from our study of the metabasite restites are placed on a P-T diagram together with available data [*Enami et al.*, 1993b; *Wang et al.*, 1993; *Zhang et al.*, 1995; *Yao et al.*, 2000; *Zhai et al.*, 2000] (Figure 12). This

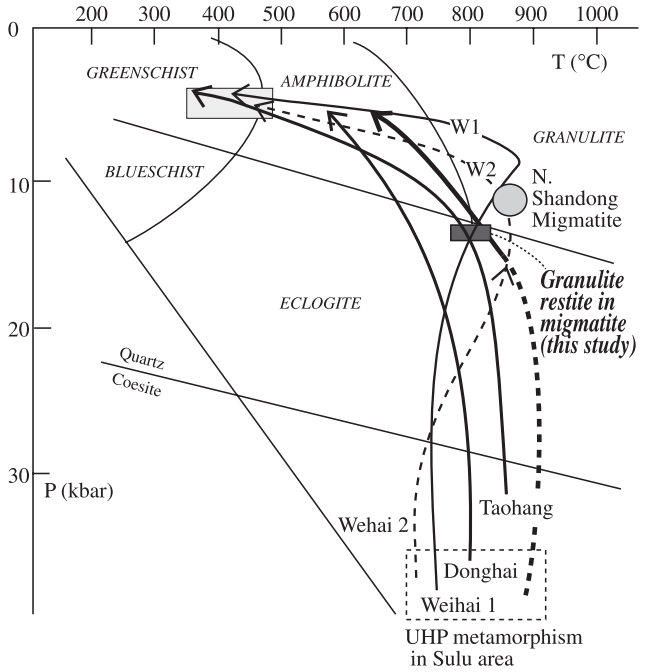

Figure 12. Synthesis of pressure-temperature paths inferred from different tectonometamorphic units of the Shandong peninsula. Most of the UHP metamorphic rocks of the Sulu area follow quite similar paths. Non-migmatized UHP rocks in Donghai [*Zhang et al.*, 1995] and Taohang [*Yao et al.*, 2000]. Thick black path is granulitized eclogite restite in migmatite from Weihai (Wehai 1 [*Zhai et al.*, 2000]; Wehai 2 [*Wang et al.*, 1993]). Granulite restite in migmatite [*Zhai et al.*, 2000; this study]. Gray circle corresponds to pressure-temperature field of migmatite north of Laiyang [*Enami et al.*, 1993b]. Light gray box corresponds to the lowest metamorphic grade.

granulitic metamorphism is followed by retrogression in amphibolite facies characterized by plagioclase-green amphibole-zoisite assemblage. In East Shandong Peninsula (Weihai area), the P-T conditions of retrogression have been estimated at 480°–350°C and 4–6 kbar [*Wang et al.*, 1993]. Similar conditions are likely for the retrogression of the North Shandong rocks. As shown in Figure 12, the P-T path proposed for all these mafic rocks exhibit quite similar trends. Except for the Donghai area where exhumation occurs under low temperature gradient, the initial UHP-eclogite facies formed during deep-seated subduction is followed by a decompression stage coeval with an increase in temperature. This event leads to the granulitization of the mafic eclogites and migmatization of the quartzo-feldspathic gneiss. Last, a general retrogression with both P and T decrease occurs during the main ductile deformation.

5. $^{40}Ar/^{39}Ar$ and U/Pb Geochronology

5.1. $^{40}Ar/^{39}Ar$ Geochronology

[35] During our fieldwork, several samples from the Shandong Peninsula were collected in order to place age constraints on the tectono-metamorphic and cooling evolu-

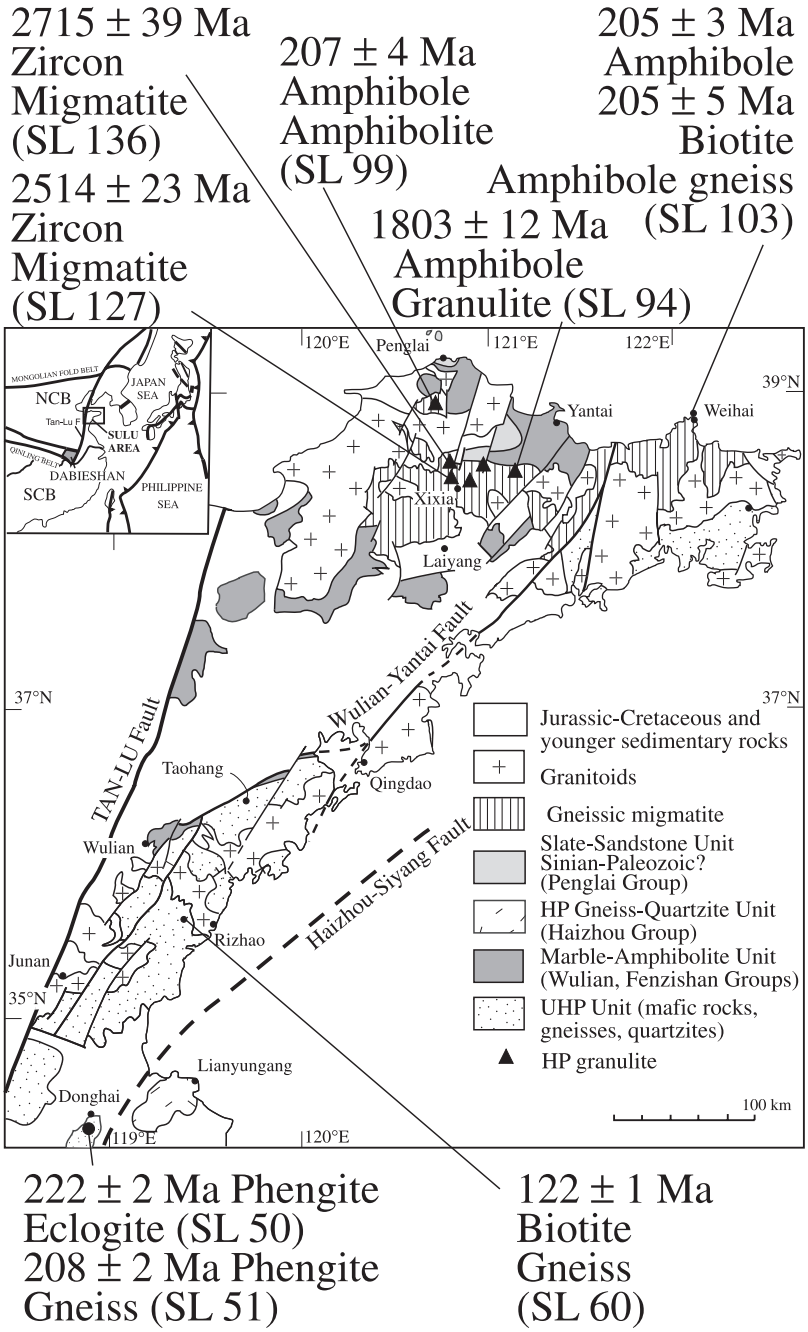

Figure 13. Location map and age results of samples used for $^{40}Ar/^{39}Ar$ geochronology in this paper; see text for discussion.

tion of the rocks exposed from the northern Shandong migmatitic domain to the southern Sulu area. These samples, located in Figure 13, include an eclogite (sample SL50) and gneisses (SL51, SL60) from southern Sulu and an amphibolite (sample SL99), a metagabbro (sample SL94) and an amphibole gneiss (sample SL103) from northern Shandong and Weihai areas which are representative of the main events recognized on structural and petrologic grounds. Minerals have been extracted from these different rocks after a coarse crushing and analyzed using the $^{40}Ar/^{39}Ar$ laser probe dating technique [*Monié et al.*, 1994; *Lin et al.*, 2000]. Argon was extracted from single grains with the laser operating in the continuous mode for step-heating experiments and in the pulsed mode for spot fusion dating. Data (Table 1) are represented as age spectra and age spot fusion maps drawn at the grain scale (Figures 14 and 15).

5.2. Results From the UHP Unit in the Sulu Area

5.2.1. Eclogite SL50

[36] This eclogite comes from Qinglungshan, near Donghai City. It is mineralogically similar to that recently studied

Table 1. $^{40}Ar/^{39}Ar$ Laser Probe Data Presented in This Paper in Figures 14 and 15[a]

Number	$^{40}Ar^*/^{39}Ar$	$^{36}Ar/^{40}Ar \times 1000$	$^{39}Ar/^{40}Ar$	$^{37}Ar/^{39}Ar$	% ^{39}Ar	% Atm	Age	Error
				SL50 Phengite Spot (*J = 0.014283*)				
1	8.882	0.606	0.0923	0	/	17.9	215.5	2.1
2	9.025	0.102	0.1074	0	/	3.0	218.8	1.4
3	9.026	0.013	0.1103	0	/	0.4	218.8	0.6
4	9.114	0.055	0.1079	0	/	1.6	220.8	1.0
5	8.765	0.389	0.1009	0	/	11.5	212.8	2.8
6	9.234	0.033	0.1072	0	/	0.9	223.5	1.1
7	9.254	0.030	0.1070	0	/	0.9	224.0	1.0
8	9.296	0.031	0.1065	0	/	0.9	224.9	1.7
9	9.210	0.030	0.1075	0	/	0.9	223.0	1.2
10	9.268	0.035	0.1067	0	/	1.0	224.3	2.8
11	9.474	0.024	0.1047	0	/	0.7	229.0	1.5
12	9.270	0.021	0.1071	0	/	0.6	224.3	1.0
13	9.131	0.016	0.1089	0	/	0.4	221.2	1.9
14	9.113	0.024	0.1089	0	/	0.7	220.8	1.5
							Total Age = 221.6 ± 2.2	
				SL51 Phengite Step (*J = 0.014283*)				
1	3.125	2.408	0.0923	0	0.1	71.1	78.8	39.5
2	9.320	0.122	0.1034	0	2.0	3.6	225.5	2.3
3	8.455	0.055	0.1163	0	5.2	1.6	205.7	1.8
4	8.937	0.049	0.1102	0	10.7	1.5	216.7	2.2
5	8.664	0.018	0.1148	0	21.8	0.5	210.5	1.4
6	8.462	0.017	0.1175	0	32.3	0.5	205.8	1.3
7	8.618	0.071	0.1136	0	35.1	2.1	209.4	2.3
8	8.538	0.009	0.1168	0	55.2	0.3	207.6	1.2
9	8.487	0.024	0.1169	0	67.0	0.7	206.4	0.8
10	8.404	0.062	0.1168	0	69.7	1.8	204.5	2.6
11	8.641	0.054	0.1138	0	73.4	1.6	210.0	0.7
12	8.452	0.055	0.1163	0	76.3	1.6	205.6	1.0
13	8.774	0.058	0.1120	0	83.4	1.7	213.0	1.9
14	8.912	0.015	0.1116	0	100.0	0.5	216.2	1.5
							Total Age = 210.1 ± 2.2	
				SL60 Biotite Spot (*J = 0.014283*)				
1	5.250	2.265	0.0629	0	/	66.9	130.5	6.8
2	4.931	1.280	0.1260	0	/	37.8	122.8	2.8
3	4.419	2.120	0.0844	0	/	62.6	110.4	2.6
4	4.373	1.589	0.1212	0	/	46.9	109.3	2.0
5	5.005	0.980	0.1418	0	/	28.9	124.6	2.8
6	4.832	1.109	0.1390	0	/	32.8	120.4	1.4
7	4.792	1.543	0.1134	0	/	45.6	119.5	2.5
8	4.917	0.491	0.1737	0	/	14.5	122.5	1.7
9	4.958	0.634	0.1638	0	/	18.7	123.4	2.2
10	5.074	0.550	0.1649	0	/	16.2	126.2	2.0
11	4.866	0.887	0.1515	0	/	26.2	121.2	1.5
12	4.710	0.552	0.1776	0	/	16.3	117.5	2.3
							Total Age = 120.3 ± 1.5	
				SL94 Amphibole Step-Heating (*J = 0.014283*)				
1	658.24	1.614	0.0006	0.000	0.0	47.6	4225.1	64.4
2	1145.20	0.489	0.0006	1.882	0.0	14.4	5148.8	86.1
3	317.10	0.224	0.0029	3.711	0.1	6.6	3085.1	53.2
4	219.46	0.078	0.0044	5.743	1.4	2.3	2560.7	12.7
5	124.97	0.023	0.0079	5.547	5.2	0.7	1847.8	10.9
6	121.01	0.016	0.0082	5.560	9.0	0.4	1810.8	5.8
7	119.92	0.022	0.0082	5.466	12.9	0.6	1800.5	5.8
8	121.17	0.023	0.0081	5.506	16.6	0.6	1812.3	5.9
9	122.67	0.012	0.0081	5.656	19.9	0.3	1826.4	6.4
10	118.87	0.012	0.0083	5.541	24.1	0.3	1790.4	8.5
11	119.24	0.013	0.0083	5.568	28.3	0.4	1794.0	8.6
12	118.87	0.018	0.0083	5.536	32.6	0.5	1790.5	5.5
13	119.75	0.014	0.0083	5.877	37.2	0.4	1798.9	4.9
14	118.28	0.010	0.0084	5.387	41.2	0.3	1784.8	7.3
15	122.15	0.030	0.0081	5.446	44.0	0.9	1821.5	15.9
16	122.34	0.007	0.0081	5.388	45.9	0.2	1823.3	10.1
17	121.35	0.011	0.0082	5.414	47.8	0.3	1814.0	11.6
18	121.14	0.020	0.0082	5.574	51.1	0.6	1812.0	9.8
19	119.62	0.006	0.0083	5.485	55.2	0.1	1797.6	5.3

Table 1. (continued)

Number	$^{40}Ar^*/^{39}Ar$	$^{36}Ar/^{40}Ar \times 1000$	$^{39}Ar/^{40}Ar$	$^{37}Ar/^{39}Ar$	% ^{39}Ar	% Atm	Age	Error
20	119.22	0.021	0.0083	5.447	59.5	0.6	1793.8	6.6
21	119.30	0.021	0.0083	5.285	63.1	0.6	1794.6	3.4
22	120.85	0.005	0.0082	5.423	66.8	0.1	1809.3	3.8
23	118.52	0.010	0.0084	5.458	70.0	0.3	1787.1	6.3
24	120.09	0.010	0.0082	5.354	74.0	0.3	1802.1	10.3
25	121.16	0.003	0.0082	5.265	75.7	0.1	1812.2	8.1
26	120.65	0.003	0.0082	5.266	79.8	0.1	1807.4	8.9
27	120.70	0.015	0.0082	5.108	83.0	0.4	1807.9	6.7
28	120.43	0.033	0.0082	5.251	85.0	0.9	1805.3	8.7
29	120.26	0.008	0.0082	5.171	88.0	0.2	1803.6	8.2
30	121.01	0.019	0.0082	5.412	89.6	0.5	1810.8	10.6
31	120.14	0.034	0.0082	5.159	91.4	1.0	1802.5	8.0
32	119.84	0.030	0.0082	5.358	93.2	0.9	1799.7	8.9
33	119.31	0.038	0.0082	5.402	95.6	1.1	1794.6	9.0
34	125.01	0.057	0.0078	6.020	96.2	1.7	1848.2	15.2
35	121.35	0.017	0.0081	6.647	100.0	0.5	1814.0	5.8
							Total Age = 1824.4 ± 12.4	
				SL99 Amphibole Spot (*J = 0.014283*)				
1	7.410	0.296	0.1231	4.061	/	8.7	181.5	3.3
2	6.654	0.463	0.1297	3.537	/	13.6	163.8	2.5
3	7.699	0.179	0.1229	5.273	/	5.3	188.2	2.8
4	7.026	0.545	0.1193	4.114	/	16.1	172.5	4.0
5	8.495	0.445	0.1022	4.564	/	13.1	206.6	4.0
6	7.433	0.186	0.1270	4.038	/	5.5	182.0	1.6
7	5.443	0.058	0.1805	5.244	/	1.7	135.1	2.1
8	7.167	0.213	0.1306	4.646	/	6.3	175.8	2.8
9	6.888	0.372	0.1291	5.514	/	11.0	169.3	1.9
							Total Age = 172.9 ± 2.0	
				SL103 Biotite Spot (*J = 0.015627*)				
1	7.617	3.076	0.0119	0.020	/	90.8	202.9	16.2
2	7.373	1.941	0.0577	0.075	/	57.3	196.8	7.0
3	7.168	1.445	0.0798	0.000	/	42.7	191.5	3.2
4	7.690	1.402	0.0761	0.000	/	41.4	204.7	5.3
5	7.424	1.443	0.0771	0.000	/	42.6	198.0	2.7
6	7.368	0.831	0.1023	0.000	/	24.5	196.6	1.8
7	7.199	0.536	0.1168	0.000	/	15.8	192.3	1.7
8	7.504	0.703	0.1055	0.000	/	20.7	200.1	2.0
9	7.670	1.118	0.0872	0.005	/	33.0	204.2	3.1
							Total Age = 199.1 ± 2.7	
				SL103 Amphibole Step-Heating (*J = 0.015627*)				
1	116.619	2.031	0.0034	2.173	0.0	60.0	1871.9	43.0
2	14.189	2.418	0.0201	1.005	0.3	71.4	361.3	20.3
3	7.462	1.159	0.0880	0.668	0.8	34.2	199.0	5.3
4	7.012	0.918	0.1038	0.400	1.8	27.1	187.6	2.8
5	8.882	0.840	0.0846	0.093	2.0	24.8	234.5	15.9
6	7.011	0.379	0.1266	0.131	2.8	11.2	187.6	3.1
7	7.168	0.237	0.1297	0.181	3.5	7.0	191.6	5.5
8	8.194	0.275	0.1121	1.180	4.9	8.1	217.4	2.2
9	8.504	0.108	0.1138	2.251	10.7	3.1	225.1	1.4
10	7.739	0.041	0.1276	2.484	24.3	1.2	206.0	1.1
11	7.745	0.040	0.1275	2.469	51.5	1.1	206.1	1.1
12	7.665	0.062	0.1279	2.043	54.8	1.8	204.1	2.3
13	7.829	0.024	0.1268	2.549	73.5	0.7	208.2	1.1
14	7.738	0.053	0.1270	2.465	83.6	1.5	206.0	0.9
15	7.540	0.090	0.1289	2.223	85.7	2.6	201.0	3.8
16	7.589	0.064	0.1292	2.487	100.0	1.9	202.2	1.0
							Total Age = 209.1 ± 1.9	

[a]The mean integrated age for spot fusion analyses results from the addition of argon isotopes for all spots within a single grain, with no normalization to the grain volume.

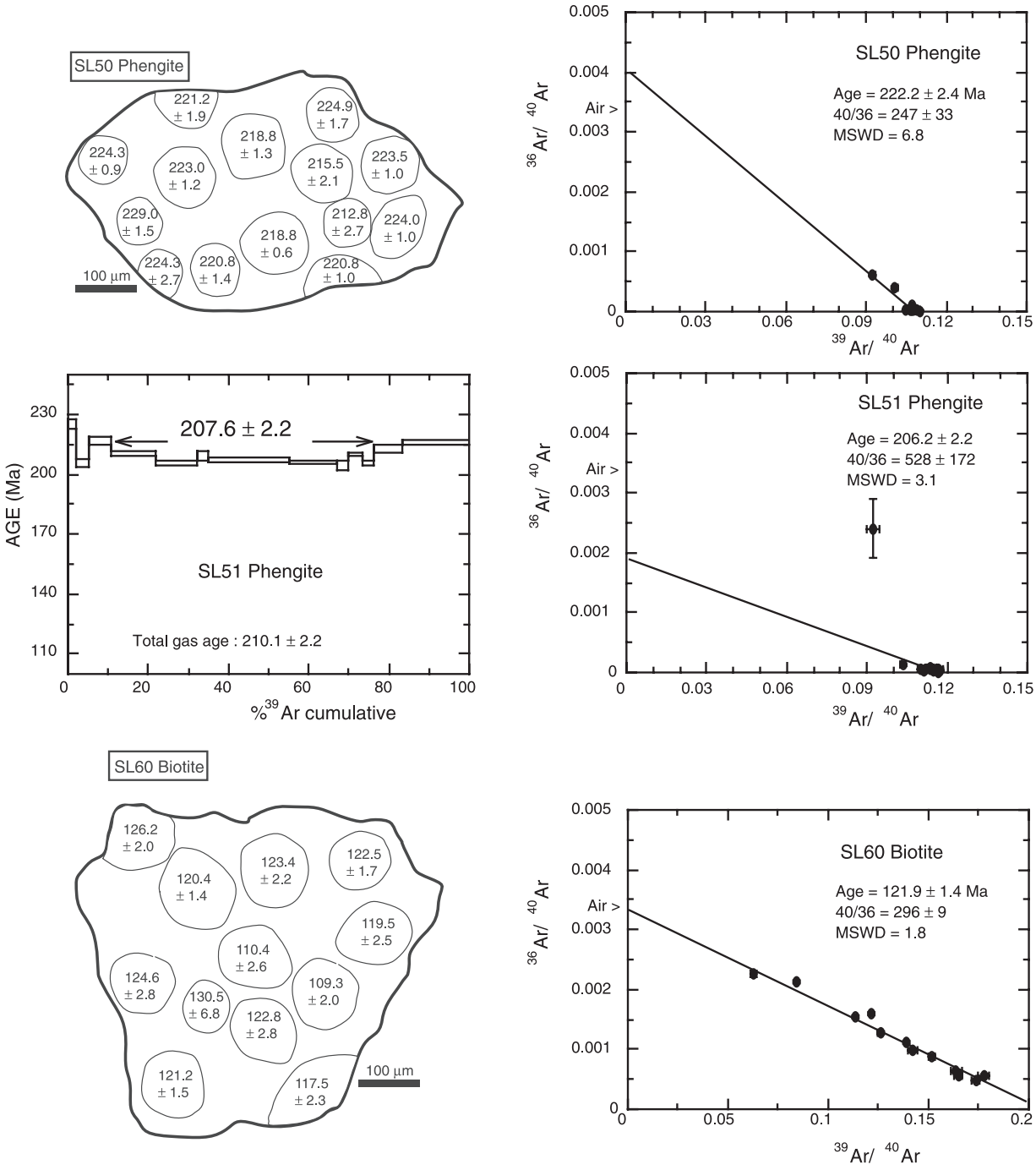

Figure 14. $^{40}Ar/^{39}Ar$ dates get for Sulu UHP Unit (see text for details).

in detail by *Giorgis et al.* [2000] with an assemblage essentially made of omphacite, kyanite, phengite, garnet and rutile. A single grain of phengite was extracted from this sample and analyzed by a series of fourteen spot fusions performed perpendicularly to the mica cleavage in order to investigate possible intragrain isotopic heterogeneities. Individual ages range from 212.8 ± 2.7 Ma to 229.0 ± 1.5 Ma (Figure 14), with no systematic age variation from the core to the rim of the grain. The isotope correlation plot $^{36}Ar/^{40}Ar$ vs. $^{39}Ar/^{40}Ar$ gives an intercept age of 222.2 ± 2.4 Ma with an initial $^{40}Ar/^{36}Ar$ ratio of 247 ± 33 (MSWD = 6.8). These results are very different from those reported by *Giorgis et al.* [2000] from the same area who found evidence of a strong contamination by inherited argon with ages up to 900 Ma.

5.2.2. Gneiss SL51

[37] A gneiss, which forms the envelope of the previous eclogite, was collected in the same area. A single phengite grain of this sample was selected for stepwise argon analysis. The age spectrum (Figure 14) displays a concave

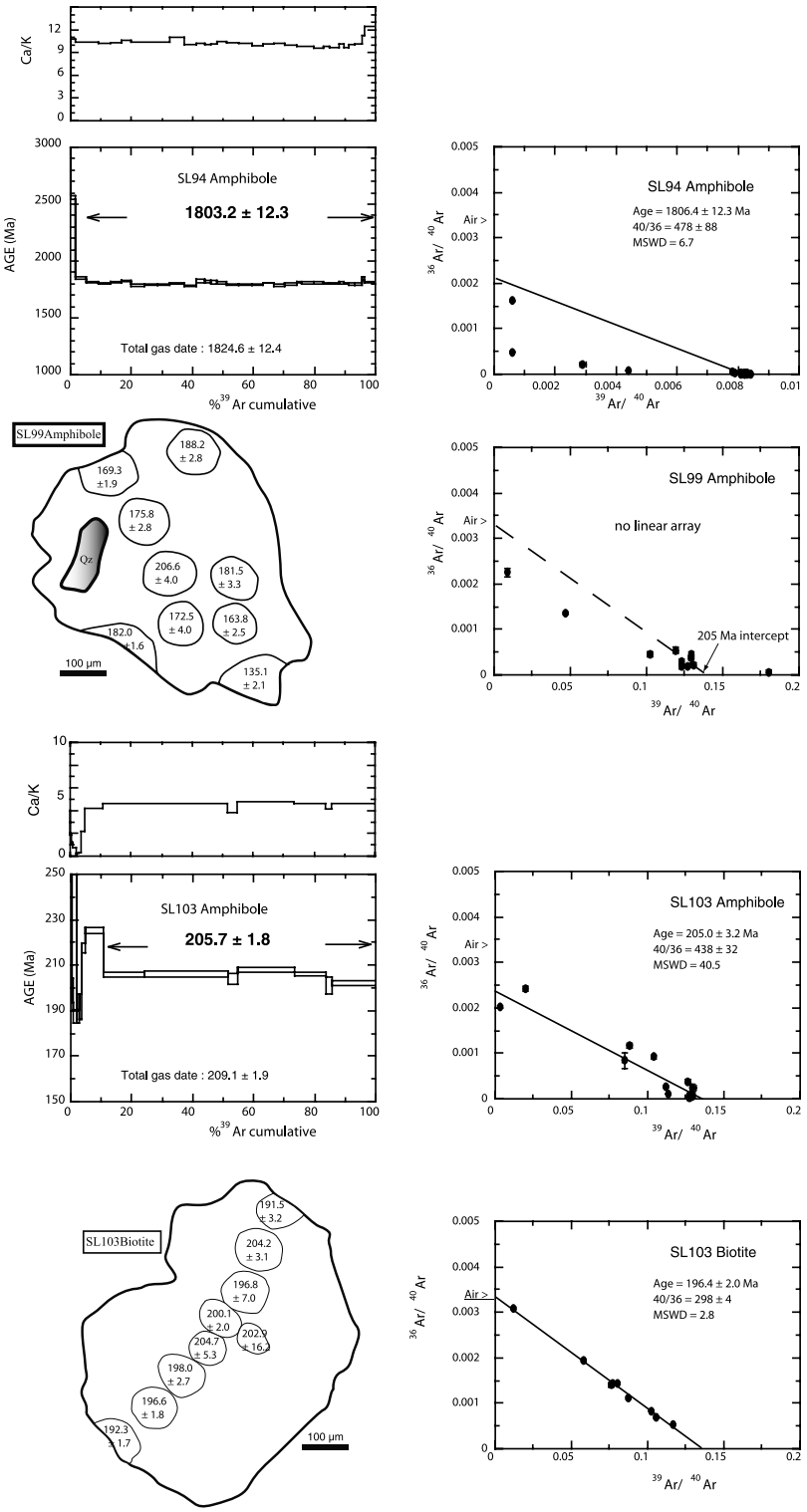

Figure 15. $^{40}Ar/^{39}Ar$ dates get for the North Shandong and Weihai areas (see text for details).

pattern with an integrated date of 207.6 ± 2.2 Ma obtained for the intermediate gas fractions representing 60% of the gas released. In the correlation plot, the data cluster near the abscissa axis with an intercept age of 206.2 ± 2.2 Ma and a poorly defined $^{40}Ar/^{36}Ar$ ratio of 528 ± 172 (MSWD = 3.1). The characteristics of the age spectrum and correlation plot suggest the presence of a minor amount of excess argon.

5.2.3. Gneiss SL60

[38] Biotite has been extracted from a well lineated augen orthogneiss containing also mafic enclaves sampled North

of Rizhao. Kinematic indicators such as sigmoidal K-feldspar and σ-type porphyroclast systems point to NW shearing during the main stage of rock exhumation. Twelve spot fusions have been achieved on the surface of a single grain (Figure 14). Ages are varying between 130.5 ± 6.8 and 109.3 ± 2.0 Ma, with a mean age of 120.3 ± 1.5 Ma. In the correlation plot, the date scatter along a single line with an intercept age of 121.9 ± 1.4 Ma and an initial argon ratio of 296 ± 9 (MSWD = 1.8). Note the relatively high atmospheric contamination of this sample compared to the previously dated phengites (Table 1).

5.3. Results From North Shandong Area

5.3.1. Granulitic Metagabbro SL94

[39] This rock with a coarse grain assemblage made of amphibole, plagioclase, garnet, clinopyroxene is similar to sample SL 95 described in section 4. It forms a metric boudin spared by the ductile deformation developed in the adjacent gneissic migmatites and amphibolites. A single grain of amphibole was progressively degassed using 35 heating increments (Figure 15). With the exception of the fourth first steps which show contamination by a weakly bound excess argon, nearly 95% of the gas released yields a plateau date of 1803.2 ± 12.3 Ma corresponding to a flat Ca/K spectrum testifying of the chemical homogeneity of the dated amphibole. The isotope correlation plot suggests a similar closure age for argon diffusion despite a strong clustering of the data points near the $^{39}Ar/^{40}Ar$ axis and a badly defined initial $^{40}Ar/^{36}Ar$ ratio (MSWD = 6.7).

5.3.2. Amphibolite SL99

[40] This garnet amphibolite which comes from S. of Penglai forms a meter-scale boudin enclosed in gneissic migmatite. Structurally, this rock is located in the ductile extensional shear zone immediately underneath the detachment fault of the Marble-Amphibolite Unit. Nine spot fusion ages have been obtained on a large amphibole crystal (Figure 15). They range from 206.6 ± 4.0 Ma in the core to 135.1 ± 2.1 Ma on the edge with no systematic variation of the Ca/K ratio (see $^{39}Ar/^{37}Ar$ ratios in Table 1) and no linear trend in the isotope correlation plot.

5.3.3. Amphibole Gneiss SL103

[41] This rock comes from Weihai area. It corresponds to a mafic boudin enclosed in a gneissic migmatite which exhibits a N100°E trending mineral lineation and top-to-the NW shear criteria. Both amphibole and biotite from this rock have been analyzed. Again with the exception of the first heating increments that seem to indicate a complex story of excess and loss of argon, about 90% of the gas released from the amphibole yields a plateau date of 205.7 ± 1.8 Ma related to constant Ca/K ratios. The data strongly scatter in the isotope correlation plot (Figure 15) as indicated by the high mean squared weighted deviation (MSWD = 40). A transect has been made on a biotite from the same sample. Apparent spot fusion ages range from about 205 to 197 Ma in the core of the mica to a minimum of 192 Ma on both edges. The data show a well-defined alignment in the isotope correlation plot with an intercept age of 196.4 ± 2.0 Ma and an initial argon ratio of 298 ± 4 (MSWD = 2.8).

5.4. Interpretation of the Geochronological Results

[42] In the Sulu area, the 222 ± 2 Ma date (SL 50) complies with already published Sm/Nd and U/Pb ages [e.g., *Li et al.*, 1993a, 1993b, 1994, 1996; *Ames et al.*, 1996; *Ishizaka et al.*, 1994; *Yang and Jahn*, 2000]. It is worth noting that in our samples, conversely to previous analyses on similar rocks [e.g., *Li et al.*, 1994; *Giorgis et al.*, 2000], no excess argon can be demonstrated. The circa 208 Ma age got from gneiss host rock of eclogite supports a recrystallization and partial resetting of the UHP phengites during the top-to-the-NW shearing that accommodates the exhumation stage. The saddle shaped spectrum indicates that the K-Ar chronometer has been incompletely reset.

[43] In the N. Shandong area, the Late Triassic (circa 200 Ma) event is recorded in both migmatites from Weihai (SL 103) and Layang areas (SL 99). In sample SL 103, the 10 Ma difference between amphibole and biotite, from 206 Ma to 196 Ma indicates an average cooling rate of 20°C/Ma derived from closure temperatures of 550°C and 350°C for amphibole and biotite, respectively. Such a figure is in agreement with a fast cooling during exhumation. The 1.8 Ga date found in the granulitic metagabbro (SL 94) can be interpreted as the age of the N. Shandong basement. It is worth to note that Paleoproterozoic ages around 1.5 to 1.6 Ga have been obtained by punctual dating on metamorphic monazite in gneissic migmatite [*Enami et al.* 1993b] (Figure 13).

[44] Last, the Cretaceous age of biotite (SL 60) is related to the thermal influence of a nearby pluton. Similar resetting is already well demonstrated in many places of Eastern China [e.g., *Eide et al.*, 1994; *Faure et al.*, 1996; *Hacker et al.*, 2000; *Lin et al.*, 2000].

5.5. SIMS U-Pb Dating of North Shandong Migmatites

[45] SL 127 and SL 136 are two foliated and lineated gneissic migmatites sampled north of Xixia (Figure 13). Those migmatites form the host rock of the granulite boudins studied in section 4. Sample SL 127 is a biotite poor quartz-K-feldspar leucosome whereas in sample SL 136 the foliation is well marked by biotite preferred orientation. Zircon grains recovered from both samples are large, euhedral, colorless to pale pink, grains with 200 to 500 μm size. The euhedral shape of most zircons suggests a magmatic origin. The cathodoluminescence images (Figure 16) show inherited core with complex thin zoning, often surrounded by clear overgrowth. In order to determine the age of these overgrowths, most of the analyses were performed on them. The SIMS dating was carried out in CRPG Nancy using a Cameca IMS 1270 instrument. The 13 kV O2 primary beam was used in the aperture illumination mode to produce spots of 30–40 μm in diameter. Detailed analytical conditions and data processing are given by *Deloule et al.* [2001]. The results are reported in Table 2, and plotted in the Concordia diagram (Figure 17) with isoplot [*Ludwig*, 1991]. The Concordia plot points out the main character of these zircon grains. they all stand close to

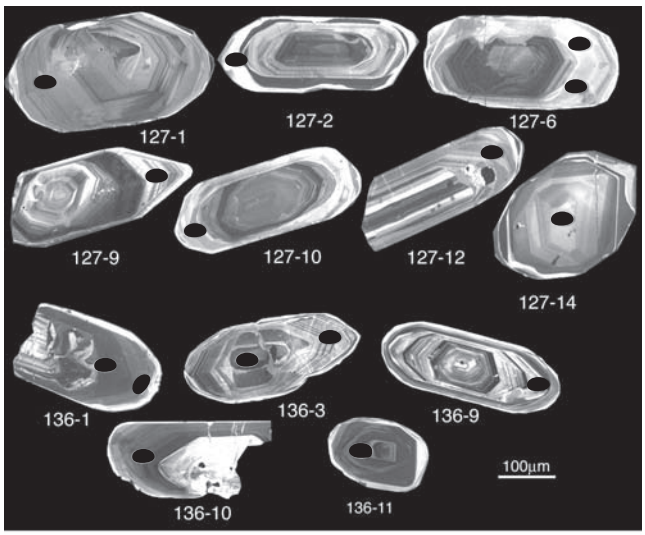

Figure 16. Cathodoluminescence images of the analyzed zircon grains from samples SL 127 and SL 136; black ellipses are the location of the analyzed areas.

the Concordia, with ages ranging from 2514 to 2831 Ma. Seven on eight data points from sample SL127 plot on a single discordia line with a MSWD of 8.1, with an upper intercept at 2514 ± 23 Ma and a lower intercept at 708 ± 860 Ma. The poor definition of the lower intercept is due to the small dispersion of the data away from the Concordia line, with discordance factors lower than 1.5% (Table 2). Five on seven data points from sample SL136 define a discordia line with a MSWD of 1.9 and upper and lower intercepts at 2715 ± 39 Ma and 1070 ± 320 Ma, respectively. The two last points plot on a discordia line intersecting the Concordia at 2831 ± 20 Ma and 808 ± 320 Ma.

[46] These results provide three different informations: (1) the inheritance of Archean and Early Proterozoic zircons attests to the implication of an old crustal segment in the subduction process; (2) the three discordia lines have a similar lower intercept poorly defined around 920 Ma, suggesting that a NeoProterozoic event took place in the North Shandong area; (3) the Triassic event, between 205–222 Ma, recorded by $^{40}Ar/^{39}Ar$ dating does not affect any of the measured zircon, although most of the measurements were done on the external rims of the grains. This suggests that for those samples, the Triassic event occurred in relatively dry conditions, with limited fluid-rocks interactions and thus preventing any zircon resetting.

6. Discussion and Conclusions

[47] The above presented structural, petrologic and geochronological data allow us to discuss the tectonic evolution of the Shandong Peninsula in the framework of the Qinling-Dabie belt and the collision between NCB-SCB. From the structural point of view, the whole peninsula,

Table 2. U-Pb Isotopic Data for the Analyzed Zircons From Samples SL 127 and SL 136[a]

Samples	$^{206}Pb/^{204}Pb$ Meas.	Pb ppm	U ppm	Th ppm	$^{207}Pb/^{206}Pb$	±	$^{207}Pb/^{235}U$	±	$^{206}Pb/^{238}U$	±	Correl.	$^{206}Pb/^{238}U$ Age	±	$^{207}Pb/^{235}U$ Age	±	$^{207}Pb/^{206}Pb$ Age	±	Discord., %
SL 127-1r1	20372	20	47	26	0.167	0.003	11.45	0.12	0.497	0.005	0.94	2602	21	2561	10	2529	6	−1.6
SL127-2r1	90827	68	162	12	0.165	0.002	11.124	0.11	0.488	0.005	0.98	2563	20	2534	9	2510	3	−1.1
SL127-6r1	25534	22	52	28	0.168	0.002	11.496	0.11	0.497	0.005	0.98	2600	20	2564	9	2536	3	−1.4
SL127-6r2	943	34	86	13	0.155	0.036	9.805	0.53	0.457	0.019	0.75	2427	82	2417	49	2408	60	−0.4
SL127-10r1	23937	31	76	11	0.168	0.003	11.062	0.11	0.478	0.005	0.96	2518	20	2528	9	2536	5	0.4
SL127-9r1	1932	55	144	8	0.164	0.004	10.013	0.11	0.443	0.005	0.93	2365	21	2436	10	2496	7	2.9
SL127-12r1	11752	17	40	18	0.165	0.003	11.608	0.11	0.509	0.005	0.95	2652	21	2573	9	2512	5	−3.0
SL127-14c	13246	9	22	18	0.166	0.003	11.273	0.119	0.491	0.004	0.95	2576	19	2546	9	2522	5	−1.2
SL136-10r1	118149	190	457	23	0.181	0.002	12.050	0.12	0.483	0.005	0.98	2542	20	2608	9	2660	3	2.5
SL136-11c	151162	229	517	31	0.186	0.005	13.281	0.15	0.517	0.005	0.91	2685	22	2700	10	2711	8	0.5
SL136-9r1	232656	242	484	180	0.203	0.007	16.323	0.32	0.583	0.011	0.93	2962	43	2896	19	2850	11	−2.3
SL136-3r1	92456	83	190	45	0.187	0.007	13.028	0.25	0.505	0.009	0.94	2634	39	2682	18	2718	11	1.8
SL136-3c1	145298	194	451	52	0.196	0.002	13.538	0.14	0.500	0.005	0.98	2615	22	2718	10	2795	3	3.8
SL136-1r1	26967	308	754	17	0.181	0.006	11.905	0.22	0.476	0.009	0.95	2508	37	2597	18	2667	10	3.4
SL136-1c	20334	172	479	28	0.173	0.003	9.967	0.11	0.419	0.005	0.97	2254	21	2432	10	2584	5	7.3

[a]Reported errors include calibration uncertainties.

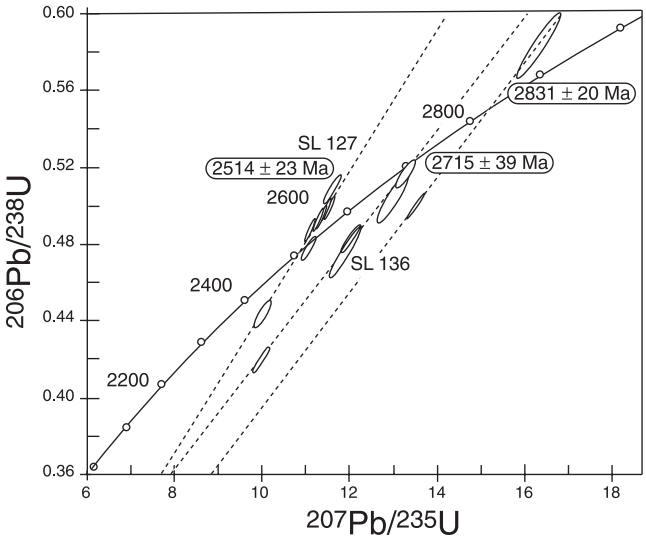

Figure 17. Concordia plots for the two foliated migmatite samples SL 127and SL 136.

including N. Shandong, Sulu, and Weihai areas, underwent the same ductile deformation. This main event, coeval with an amphibolite facies metamorphism is characterized by a NW-SE trending stretching lineation with top-to-the-NW shearing. A similar kinematic picture is recognized all over the Dabieshan and Zhangbaling area [e.g., *Hacker et al.*, 1995, 2000; *Faure et al.*, 1999, 2003; W. Lin et al., Polyphase deformation in the Feidong-Zhangbaling Massif (eastern China) and its place in the collision between the North China and South China Blocks title, submitted to *Asian Journal of Earth Sciences*, 2003] (Figure 1).

[48] In Shandong Peninsula, all the tectonic units separated by low angle extensional detachment faults experienced the same shearing which is dated by our $^{40}Ar/^{39}Ar$ measurements around 210–205 Ma, i.e., Late Triassic. Moreover, this extensional tectonics is preceded by top-to-the-south ductile shearing recorded in blueschist facies metamorphic rocks near Lianyungang, in the southernmost part of the study area (Figure 2). This Early Triassic top-to-the-south event is also reported from the Zhangbaling area where it is dated between 245 and 212 Ma by $^{40}Ar/^{39}Ar$ on blue amphibole and phengite [e.g., *Wang et al.*, 1996; *Chen et al.*, 1992, 2000], and in the southern part of the Dabieshan [*Eide et al.*, 1994; *Wang et al.*, 1998; *Faure et al.*, 1999, 2003; *Hacker et al.*, 2000]. Since this Early Triassic HP metamorphism is coeval with southward shearing, this event is considered as a compressional one. At depth, southward thrusting in the Shandong Peninsula is also supported by a seismic profile that shows northward dipping reflectors interpreted as thrust surfaces [*Yang*, 2000]. However, the geodynamic setting of the Triassic tectonics is not clearly settled yet. It is generally acknowledged that the HP metamorphism is due to the NCB-SCB collision. Nevertheless, several controversial points arise.

[49] Our structural and petrologic study shows that the whole Shandong Peninsula experienced the same geodynamic evolution. As already emphasized [*Faure et al.*, 2001], since similar lithologies, structures and metamorphic events can be clearly observed on both sides of the central Shandong Cretaceous basin, geological evidence for a major Triassic plate boundary between N. Shandong and Sulu-Weihai areas is completely lacking. Although the Sulu and Weihai eclogites are considered as quite distinct from the North Shandong HP granulites [e.g., *Zhai et al.*, 2000], several lines of evidence support a correlation between those three areas. First, it has been demonstrated in several places of the Sulu area, that UHP eclogites are overprinted by a granulite facies metamorphism with 700°–800°C and 0.7–1.2 Gpa conditions [*Nakamura and Hirajima*, 2000; *Yao et al.*, 2000]; Second, in Weihai, the UHP eclogites occur as meter-size blocks enclosed within gneissic migmatites, thirdly, the Weihai UHP eclogites also experienced a granulite facies overprint [*Wang et al.*, 1993] (Figure 12). Last, on the basis of Nd geochemistry and geochronology, a HP and HT event at circa 1.7 Ga is recognized in the Weihai migmatite [*Jahn et al.*, 1996]. The main difference between North Shandong and Sulu areas is that in the latter, the high temperature overprint is weak and thus the earlier UHP metamorphism is better preserved. It is worth to note that a similar evolution is reported from the Dabieshan. There, granulite blocks are described in gneissic migmatite [e.g., *Zhang et al.*, 1996] and eclogite xenoliths are recovered in Cretaceous granites intruding the migmatite [*Faure et al.*, 1999, 2003]. Consequently, in this paper we propose that the Shandong Peninsula as a whole belong to SCB. In this interpretation, the granulite facies metamorphism would correspond to the retrogression during the exhumation of mafic UHP metamorphic rocks. Due to their more aluminous composition and probably high fluid content, the granitoids and their pelitic host rocks are easily melted and give rise to the migmatites into which the mafic rocks are enclosed.

[50] Although very attractive and simple, the assumption that blueschist facies metamorphism is coeval with the eclogite facies metamorphism is another disputable point in previous interpretations. Indeed, the Triassic radiometric dates of the Sulu and Dabieshan eclogites as those of the real age of the UHP metamorphism can be questioned. As well acknowledged, the closure of the U-Pb and Sm-Nd geochronometers (and less robust Rb-Sr and K-Ar) is mostly controlled by thermal diffusion and mineral recrystallization rather than pressure. Petrology shows that pressure and temperature climax are not reached at the same time, since pressure peak corresponds to the crystallization of coesite and other UHP minerals whereas temperature climax was reached during the granulite facies overprint and migmatization related to the exhumation stage. Therefore ages of 220–240 Ma attributed to the UHP metamorphism (cf. *Ayers et al.* [2002] for one of the most recent works) do not necessarily correspond to the pressure peak.

[51] The reality of a Triassic event, called "Indosinian orogeny," is well recognized for a long, even if not well understood yet. In particular, the relationships between the

Qinling-Dabieshan massif and Shandong Peninsula; and the pre-Cretaceous role of the Tan-Lu fault either as a suture zone, transfer fault or late structure [e.g., *Xu et al.*, 1987; *Okay et al.*, 1993; *Yin and Nie*, 1993; *Gilder et al.*, 1999] is beyond the scope of this paper. The study of the Shandong Peninsula provides additional data to support a Triassic southward compression coeval with blueschist facies metamorphism followed by top-to-the-NW exhumation. In terms of geodynamics, this Triassic event remains to be fully deciphered. Presently, in agreement with *Mattauer et al.* [1985], we consider that the Triassic orogeny of Central China corresponds to intracontinental tectonics unrelated to the UHP metamorphism. In the present state of knowledge, an integrated geodynamic evolution model for the Shandong Peninsula appears premature. Nevertheless an Early Paleozoic or even older age for the UHP metamorphism and the NCB-SCB collision cannot be merely discarded.

[52] **Acknowledgments.** Field and laboratory expenses have been supported by a Chinese MOST grant G1999 043303, Major State Basic Research Development Project of China (G1999075506), a French CNRS Intérieur de la Terre project, and by a Franco-Chinese Cooperation Foundation (AFCRST-PRA T03). A post-doctorate grant for Wei Lin from the Conseil Regional du Centre (France) is also acknowledged.

References

Ames, L., G. Zhou, and B. Xiong, Geochronology and isotopic character of ultra high-pressure metamorphism with implications for collision of the Sino-Korean and Yangtze cratons, central China, *Tectonics*, *15*, 472–489, 1996.

Ayers, J. C., S. Dunkle, S. Gao, and C. F. Miller, Constraints on timing of peak and retrograde metamorphism in the Dabie Shan ultrahigh-pressure metamorphic belt, east-central China, using U-Th-Pb dating of zircon and monazite, *Chem. Geol.*, *186*, 315–331, 2002.

Chen, W., T. M. Harrison, M. T. Heizler, R. Liu, B. Ma, and J. Li, The cooling history of melange zone in north Jiangsu-south Shandong region: Evidence for multiple diffusion domain $^{40}Ar/^{39}Ar$ thermal geochronology, *Acta Petrol. Sin.*, *8*, 1–17, 1992.

Chen, X., X. Wang, and Q. Zhang, Geochronologic study on the formation and evolution of Tan-Lu fault (in Chinese), *J. Changchun Univ. Sci. Technol.*, *30*, 215–220, 2000.

Cong, B., (Ed.), *Ultrahigh-Pressure Metamorphic Rocks in the Dabieshan-Sulu Region of China*, 224 pp., Kluwer Acad., Norwell, Mass., 1996.

Deloule, E., P. Alexandrov, A. Cheilletz, B. Laumonier, and P. Barbey, In situ U-Pb zircon ages for Early Ordovician magmatism in the Eastern Pyrénées, France: The Canigou orthogneisses, *Int. J. Earth Sci.*, *91*, 398–405, 2001.

Eide, E. A., M. O. McWilliams, and J. G. Liou, $^{40}Ar/^{39}Ar$ geochronology and exhumation of high-pressure to ultrahigh-pressure metamorphic rocks in east-central China, *Geology*, *22*, 601–604, 1994.

Ellis, D. J., and D. H. Green, An experimental study of the effect of Ca upon Garnet-Clinopyroxene Fe-Mg exchange equilibria, *Contrib. Mineral. Petrol.*, *71*, 13–22, 1979.

Enami, M., and Q. Zhang, Quartz pseudomorph after coesite in eclogite from Shandong province, East China, *Am. Mineral.*, *75*, 381–386, 1990.

Enami, M., Q. Zhang, and Y. Yin, High-pressure eclogites in northern Jiangsu-southern Shandong province, eastern China, *J. Metamorph. Geol.*, *11*, 589–603, 1993a.

Enami, M., K. Suzuki, M. Zhai, and X. Zheng, The chemical Th-U-total Pb isochron ages of Jiaodong and Jiaonan metamorphic rocks in the Shandong Peninsula, eastern China, *Island Arc*, *2*, 104–113, 1993b.

Faure, M., Y. Sun, L. Shu, P. Monié, and J. Charvet, Extensional tectonics within a subduction-type orogen: The case study of the Wugongshan dome (Jiangxi Province SE China), *Tectonophysics*, *263*, 77–108, 1996.

Faure, M., W. Lin, L. Shu, Y. Sun, and U. Schärer, Tectonics of the Dabieshan (Eastern China) and possible exhumation mechanism of ultra-high pressure rocks, *Terra Nova*, *11*, 251–258, 1999.

Faure, M., W. Lin, and N. Le Breton, Where is the North China-South China block boundary in eastern China?, *Geology*, *29*, 119–122, 2001.

Faure, M., W. Lin, U. Schärer, L. Shu, Y. Sun, and N. Arnaud, Continental subduction and exhumation of UHP rocks: Structural and geochronological insights from the Dabieshan (E. China), *Lithos*, in press, 2003.

Gilder, S., P. H. Leloup, V. Courtillot, Y. Chen, S. R. Coe, X. Zhao, W. Xiao, N. Halim, J.-P. Cogné, and R. Zhu, Tectonic evolution of the Tancheng-Lujiang (Tan-Lu) fault via Middle Triassic to early Cenozoic paleomagnetic data, *J. Geophys. Res.*, *104*, 15,365–15,390, 1999.

Giorgis, D., M. Cosca, and S. Li, Distribution and significance of extraneous argon in UHP eclogite (Sulu terrain, China): Insight from in situ $^{40}Ar/^{39}Ar$ UV-laser ablation analysis, *Earth Planet. Sci. Lett.*, *181*, 605–615, 2000.

Hacker, B. R., L. Ratschbacher, L. Webb, and S. Dong, What brought them up?: Exhumation of the Dabie shan ultrahigh-pressure rocks, *Geology*, *23*, 743–746, 1995.

Hacker, B. R., L. Ratsbacher, L. Webb, T. Ireland, A. Calvert, S. Dong, R.-H. Wenk, and D. Chateigner, Exhumation of the ultrahigh- pressure continental crust in east-central China: Late Triassic-Early Jurassic extension, *J. Geophys. Res.*, *105*, 13,339–13,364, 2000.

Hirajima, T., A. Ishiwatari, B. Cong, R. Zhang, S. Banno, and T. Nozaka, Coesite from Menzhong eclogite at Donghai County, northeastern Jiangsu Province, China, *Mineral. Mag.*, *54*, 579–583, 1990.

Hirajima, T., S. Wallis, M. Zhai, and K. Ye, Eclogitized metagranitoid from the Su-Lu ultra-high pressure province, eastern China, *Proc. Jpn. Acad.*, *69*, 249–254, 1993.

Ishizaka, K., T. Hirajima, and X. Zheng, Rb-Sr dating for the Jiaodong gneiss of the Sulu ultra high-pressure province eastern China, *Island Arc*, *3*, 232–241, 1994.

Jahn, B. M., Sm-Nd isotope tracer study of UHP metamorphic rocks: Implications for continental subduction and collisional tectonics, *Int. Geol. Rev.*, *41*, 859–885, 1999.

Jahn, B. M., J. Cornichet, B. Cong, and T. Yui, Ultrahigh ε_{Nd} eclogites from an ultrahigh-pressure metamorphic terrane of China, *Chem. Geol.*, *127*, 61–79, 1996.

Ji, Z., and H. Zhao, New evidence for the age of the Penglai group in Ludong (in Chinese), *J. Stratigr.*, *16*, 237–238, 1992.

Kato, T., M. Enami, and M. Zhai, Ultra-high-pressure marble and eclogite in the Su-Lu UHP terrane, eastern China, *J. Metamorph. Geol.*, *15*, 169–182, 1997.

Krogh, E. J., The garnet-clinopyroxene Fe-Mg geothermometer- a reinterpretation of existing experimental data, *Contrib. Mineral. Petrol.*, *99*, 44–48, 1988.

Law, R. D., Crystallographic fabrics: A selective review of their applications to research in structural geology, in *Deformation Mechanisms, Rheology and Tectonics*, edited by R. J. Knipe and E. H. Rutter, *Geol. Soc. Spec. Publ.*, *54*, 335–352, 1990.

Leake, B. A., J. C. Schumacher, N. C. N. Stephenson, L. Ungaretti, E. J. W. Whittaker, and G. Youzhi, Nomenclature of amphiboles, Report of the subcommittee on Amphiboles of the International Mineralogical Association Commission on the New Mineral Names, *Can. Mineral.*, *9*, 623–651, 1997.

Li, S., et al., Collsion of North China and Yangtze Blocks and formation of coesite-bearing eclogites: Timing and processes, *Chem. Geol.*, *109*, 89–111, 1993a.

Li, S., D. Liu, and Y. Chen, Time of the blueschist belt formation in Central China (in Chinese), *Sci. Geol. Sin.*, *28*, 21–27, 1993b.

Li, S., S. Wang, Y. Chen, D. Liu, J. Qiu, H. Zhou, and Z. Zhang, xcess argon in phengite from eclogite, Evidence from dating of eclogite minerals by Sm-Nd, Rb-Sr and $^{40}Ar/^{39}Ar$ methods, *Chem. Geol.*, *112*, 343–350, 1994.

Li, S., E. Jagoutz, Y. Xiao, N. Ge, and Y. Chen, Chronology of ultrahigh-pressure metamorphism in the Dabie mountains and Su-Lu terrane: I. Sm-Nd isotope system, *Sci. China, Ser. D*, *39*, 597–609, 1996.

Lin, W., M. Faure, P. Monié, U. Schärer, L. Zhang, and Y. Sun, Tectonics of SE China: New insights from the Lushan massif (Jiangxi Province), *Tectonics*, *19*, 852–871, 2000.

Ludwig, K. R., Isoplot, a plotting and regression program for radiogenic isotope data, *U.S. Geol. Surv. Open File Rep.*, 91–445, 1991.

Mattauer, M., P. Matte, J. Malavieille, P. Tapponnier, H. Maluski, Z. Xu, Y. Lu, and Y. Tang, Tectonics of the Qinling Belt: Build-up and evolution of Eastern Asia, *Nature*, *317*, 496–500, 1985.

Mattauer, M., P. Matte, H. Maluski, Z. Xu, Q. Zhang, and Y. Wang, La limite Chine du Nord-Chine du Sud au Paléozoïque et au Trias: Nouvelles données structurales et radiométriques dans le massif du Dabieshan (chaîne des Qinling), *C. R. Acad. Sci. Paris*, *312*, 1227–1233, 1991.

Moescher, D. P., E. J. Essene, and L. M. Anovitz, Calculation and application of clinopyroxene-garnet-plagioclase-quartz geobarometers, *Contrib. Mineral. Petrol.*, *100*, 92–106, 1988.

Monié, P., J. Soliva, M. Brunel, and H. Maluski, Les cisaillements mylonitiques du granite de Millas (Pyrénées, France): Age crétacé $^{40}Ar/^{39}Ar$ et interprétation tectonique, *Bull. Soc. Géol. Fr.*, *165*, 559–571, 1994.

Nakamura, D., and T. Hirajima, Granulite-facies overprinting of ultrahigh-pressure metamorphic rocks, Northeastern Su-Lu region, Eastern China, *J. Petrol.*, *41*, 563–582, 2000.

Newton, R. C., and D. Perkins, Thermodynamic calibration of geobarometers based on the assemblage garnet-plagioclase-orthopyroxene (clinopyroxene)-quartz, *Am. Mineral.*, *67*, 203–222, 1982.

Okay, A., A. M. C. Sengor, and M. Satir, Tectonics of an ultrahigh-pressure metamorphic terrane: The Dabieshan/Tongbaishan orogen, China, *Tectonics*, *12*, 1320–1334, 1993.

Pattison, D. R., and R. C. Newton, Reversed experimental calibration of the garnet-clinopyroxene Fe-Mg exchange thermometer, *Contrib. Mineral. Petrol.*, *101*, 87–103, 1989.

Perkins, D., Thermometry and barometry of mafic granulites based on garnet-clinopyroxene-plagioclase-quartz assemblage, *Math. Phys. Sci.*, *311*, 349–435, 1990.

Shandong Bureau of Geology and Mineral Resources (SBGMR), *Regional Geology of Shandong Province*, 639 pp., Geol. Publ., Beijing, 1991.

Wallis, S., A. Ishiwatari, T. Hirajima, K. Ye, J. Guo, D. Nakamura, T. Kato, M. Zhai, M. Enami, S. Cong, and S. Banno, Occurrence and field relationships of ultrahigh-pressure metagranitoid and coesite eclogite in the Sulu terrane, eastern China, *J. Geol. Soc. London*, *154*, 45–54, 1997.

Wallis, S., M. Enami, and S. Banno, The Sulu UHP Terrane: A review of the petrology and structural geology, *Int. Geol. Rev.*, *41*, 906–920, 1999.

Wang, Q., A. Ishiwatari, Z. Zhao, T. Hirajima, N. Hiramatsu, M. Enami, M. Zhai, and C. Cong, Coesite bearing granulite retrograded from eclogite in Weihai, eastern China, *Eur. J. Mineral.*, *5*, 141–152, 1993.

Wang, X., Z. Li, and Q. Zhang, Tectonic features of the middle part of the Tan-Lu fault zone, Field Trip Guide, *Proc. Int. Geol. Congress 30th*, 60 pp., 1996.

Wang, X., F. Neubauer, J. Genser, and W. Yang, The Dabie UHP unit, Central China: A Cretaceous extensional allochthon superposed on a Triassic orogen, *Terra Nova*, *10*, 260–267, 1998.

Xu, J., G. Zhu, W. Tong, K. Cui, and Q. Liu, Formation and Evolution of The Tancheng-Lujiang wrench fault system: A major shear system to the northwest Pacific Ocean, *Tectonophysics*, *134*, 273–310, 1987.

Yang, J., and B. M. Jahn, Deep subduction of mantle derived garnet peridotites from the Su-Lu UHP metamorphic terrane in China, *J. Metamorph. Geol.*, *18*, 167–180, 2000.

Yang, J., G. Godard, J. R. Kienast, Y. Lu, and J. Sun, Ultrahigh pressure (60 kbar) magnesite-bearing garnet peridotite from northeastern Jiangsu, China, *J. Geol.*, *101*, 541–554, 1993.

Yang, W., Analysis of deep intracontinental subduction, *Episodes*, *23*, 20–24, 2000.

Yao, Y., K. Ye, J. Liu, B. Cong, and Q. Wang, A transitional eclogite-to high pressure granulite-facies overprint on coesite-eclogite at Taohang in the Sulu ultrahigh-pressure terrane, Eastern China, *Lithos*, *52*, 109–120, 2000.

Yin, A., and S. Nie, An indentation model for the north and south China collision and the development of the Tan-Lu and Honam fault systems, eastern China, *Tectonics*, *12*, 801–813, 1993.

Zhai, M., B. Cong, J. Guo, W. Liu, Y. Li, and Q. Wang, Sm-Nd geochronology and petrography of garnet pyroxene granulites in the northern Sulu region of China and their geotectonic interpretation, *Lithos*, *52*, 23–33, 2000.

Zhang, R. Y., J. G. Liou, and B. Cong, Petrogenesis of garnet-bearing ultramafic rocks and associated eclogites in the Su-Lu ultrahigh-pressure metamorphic terrane, eastern China, *J. Metamorph. Geol.*, *12*, 169–186, 1994.

Zhang, R. Y., T. Hirajima, S. Banno, B. Cong, and J. G. Liou, Petrology of ultrahigh-pressure rocks from the southern Su-Lu region, eastern China, *J. Metamorph. Geol.*, *13*, 659–675, 1995.

Zhang, R. Y., J. G. Liou, and C. H. Tsai, Petrogenesis of a high-temperature metamorphic terrane: A new tectonic interpretation for the north Dabieshan, central China, *J. Metamorph. Geol.*, *14*, 319–333, 1996.

Zhang, R. Y., J. G. Liou, Y. Yang, and T. F. Yui, Petrochemical constraints for dual origin of garnet peridotites from Dabie-Sulu UHP terrane, eastern-central China, *J. Metamorph. Geol.*, *18*, 149–166, 2000.

E. Deloule, Centre de Recherches Petrographiques et Geochiminique and Centre National de la Recherche Scientifique (CRPG-CNRS), BP 20, F-54501 Vandoeuvre-les-Nancy, Cedex, France.

N. Le Breton, M. Faure, D. Panis, and S. Poussineau, Institut des Sciences de la Terre d'Orléans, UMR 6113, Université d'Orléans, F-45067 Orléans, Cedex 2, France. (Michel.Faure@univ-orleans.fr)

W. Lin, Institute of Geology and Geophysics, Chinese Academy of Sciences, P.O. Box 9825, 100029 Beijing, China.

P. Monié, Laboratoire de Géophysique, Tectonique et Sédimentologie, Université des Sciences et Techniques du Languedoc, Pl. E.-Bataillon, F-34095 Montpellier, Cedex, France.